CCMS-85-12

VIRGINIA TECH

CENTER FOR COMPOSITE MATERIALS AND STRUCTURES

Fatigue Damage in Notched Composite Laminates under Tension–Tension Cyclic Loads

W.W. Stinchcomb K.L. Reifsnider
E.G. Henneke G.R. Kress

September 1985

Virginia Polytechnic Institute and State University
Blacksburg, Virginia 24061

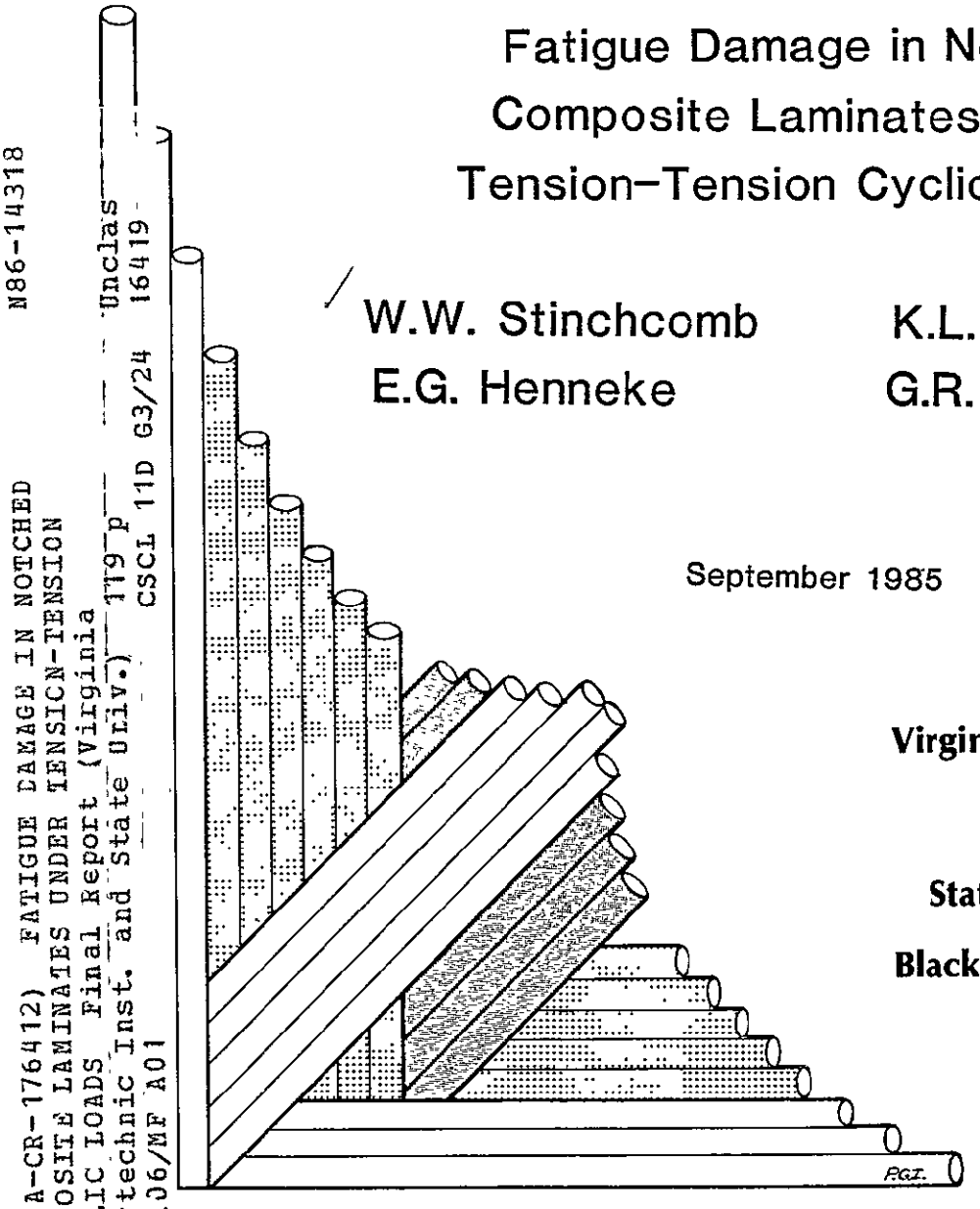

COLLEGE OF ENGINEERING

VIRGINIA POLYTECHNIC INSTITUTE AND STATE UNIVERSITY

Blacksburg, Virginia 24061

ENGINEERING SCIENCE AND MECHANICS

703/961-5259

October 31, 1985

Dr. T. K. O'Brien
MS 188E
NASA Langley Research Center
Hampton, Virginia 23665

Dear Kevin:

Enclosed, please find 3 copies of the report "Fatigue Damage in Notched Composite Laminates Under Tension-Tension Cyclic Loads." This is the final report for NASA Grant NAG-1-232.

Results from the program have been presented at the US/Japan Conference on Composite Materials sponsored by ASTM and NASA Langley (June, 1983) and have been published in ASTM Special Technical Publication 864, Recent Advances in Composite Materials in the United States and Japan. Also, data developed on this program was used to evaluate a new, and very promising, transducer to measure acoustic emission. Copies of the technical paper reporting the results of that study are also included.

We thank you for the opportunity to conduct this investigation under the sponsorship of NASA Langley.

Sincerely,

W. W. Stinchcomb
Professor

enclosures

WWS/bw

College of Engineering
Virginia Polytechnic Institute and State University
Blacksburg, Virginia 24061-4899

Fatigue Damage in Notched Composite Laminates Under Tension-Tension Cyclic Loads

W. W. Stinchcomb* K. L. Reifsnider*
E. G. Henneke* G. R. Kress**

Department of Engineering Science and Mechanics
September 1985

Final Report
Grant number NAG-1-232

Prepared for: NASA Langley Research Center
Hampton, Virginia 23665

* Professor, Engineering Science and Mechanics

** Researcher, Institute for Structural Mechanics, DFVLR, Braunschweig, West Germany. Formerly, Graduate Research Assistant, Engineering Science and Mechanics Department, Virginia Tech.

Abstract

Composite materials are established as reliable and efficient materials for a large number of structural applications. Although composites have gained a widespread use, we do not, as yet, have a precise and complete understanding of the mechanisms of damage development in composite materials. Recent research results have pointed out the need to treat damage as a collective condition; i.e., a damage state, rather than as an assembly of discrete and independent damage modes. The process of the development of the damage state and the subsequent response of the composite laminate throughout the loading history can then be related.

This report presents the results of an investigation to determine the damage states which develop in graphite epoxy laminates with center holes due to tension-tension cyclic loads, to determine the influence of stacking sequence on the initiation and interaction of damage modes and the process of damage development, and to establish the relationships between the damage states and the strength, stiffness, and life of the laminates. Two quasi-isotropic laminates were selected to give different distributions of interlaminar stresses around the hole. The laminates were tested under cyclic loads (R=0.1, 10 Hz) at maximum stresses ranging between 60 and 95 percent of the notched tensile strength. Damage was monitored

nondestructively throughout the loading history using stereo X-ray radiography, acoustic emission monitoring, and stiffness change. Some specimens were deplied after specific numbers of cycles to determine the nature and distribution of damage in each ply around the hole and to confirm the components and size of the damage state observed nondestructively. Fatigue life and residual strength tests were also performed.

Fatigue damage in the two laminates included matrix cracks in all plies followed by delaminations. The density of matrix cracks and the distribution of the damage zone (matrix cracks plus delaminations) in laminates cycled at the same percent of notched tensile strength were strongly dependent on the local constraint and distribution of interlaminar stresses as governed by the stacking sequence. The distinctly different damage states which developed in the two initially quasi-isotropic laminates due to similar load histories produced stiffness changes of 15-20 percent, different rates of residual strength degradation, and a factor of four difference in fatigue life.

The results of this study are interpreted to establish relationships between the loading history, the progressive development of the damage state, and the response of the notched laminates.

TABLE OF CONTENTS

LIST OF FIGURES

I

1.0 INTRODUCTION

Composite materials hve gained widespread use and increased consideration for primary and secondary structures in aircraft and other vehicles. These stiff, strong, light-weight materials can be used to effect decreases in weight and increases in the durability of such structures. If these advantages are to be fully realized, however, it must be possible to meet specific design requirements for aircraft and space structures. We do not, as yet, have a precise or complete understanding of the mechanisms of damage development in composite materials. Mechanisms have been identified and studied in a fragmented and casual way. Lists of the contributors to damage (such as fiber breakage, matrix cracking, debonding, delamination, etc.) are commonly made and fracture modes are frequently described in a general way.

To develop a more complete understanding of the response of composite laminates, a unified, coherent, and concentrated investigation of damage processes (not just damage components) must be made. The general objective of the experimental phase of these investigations should be to identify a well defined damage state (or states) which are

characteristic of the material response, i.e., a state which is defined by the material properties and parameters, primarily. It is also necessary to determine how this state (or states) develops into a fracture event or produces the other aspects of behavior of engineering concern during service.

Modeling depends greatly on both investigative endeavors. A model of response cannot be well set if the damage state is not well defined. Models of fatigue damage, residual strength, and stiffness degradation for unnotched laminates [1,2] are based on uniform distributions of damage that are reflected by terms such as 'characteristic damage state (CDS)', for example. These uniformities of damage do not exist in a global sense, however, in notched laminates where the stress state and the damage state associated with the notch are local, nonhomogeneous, and complex. All the modes of damage normally found under tensile loading conditions are present and combine in ways related to the local geometry and states of stress. For example, the local stress state is very complex, nearly always three-dimensional for angle ply laminates, even when the applied stress is unidirectional. And, of course, there are always sharp gradients of stress in the neighborhood of a stress raiser. Given the inherent complexity of composite materials, and the complex-

ity of the stress state at a notch, it is not too surprising to find that an understanding of fatigue damage in notched laminates is incomplete.

The objectives of the present work are to determine the nature of damage induced in graphite epoxy laminates with center holes by cyclic tensile loading and to establish the influence of such damage on the strength, stiffness and life of the laminates.

The complexity of damage mechanisms in composite materials requires complementary inspection techniques for complete description of the damage state.

Sendeckyj [3] found that the X-ray technique makes damage, namely matrix cracks and delaminations, visible but is restricted in observing spatial distribution of damage. The deply technique [4] complements the X-ray radiography because of its ability to identify specific planes of delamination. In the same sense electron microscopy can detect fiber cracks as well as the results of debonding; that is, the pullout of fibers at fracture surfaces. X-ray radiography and deply technique are different in the sense that the former is a nondestructive test (NDT) method while the latter inevitably destroys the test specimen.

Damage events during the loading process can be detected by acoustic emission recording. It yields, in combination

with the simultaneously recorded load-strain curve, information on the load and strain levels at which damage occurs; however, attempts to determine the contributing damage modes through analysis of acoustic emission signals have not been successful.

Since the strain field in notched specimens is nonuniform, it is difficult to decide what strain measurement technique gives the most valuable information. However, the moire technique [5] provides insight into the complete nonhomogeneous in-plane strain field. Furthermore, the moire technique can be applied to damaged laminates to determine changes in the local strain field. When moire data are used in conjunction with other NDT data, the effects of various damage modes on laminate response can be measured [6]. A widely used investigative method measures stiffness change as an indicator of damage in materials [7]. Camponeschi and Stinchcomb [8] pointed out that a quasi-isotropic laminate exhibits a different response than its constituent sublaminates. For instance, the response of a $[0,90,+45,-45]_s$ laminate cannot be predicted by knowing the behavior of the $[0,90]_s$ and the $[45,-45]_s$ sublaminates. In contrast, if predictions for the response of yet untested laminates are desired, they should be based on considerations like stress analyses including edge effects and constraint effects.

For designing as well as for research purposes many stress analyses for laminates with notches have been developed. Satisfactory stress analyses which account for hole related edge effects require either finite element models with many degrees of freedom, thus demanding sophisticated economical storage and computation techniques, or the skillful use of simplifying assumptions that lead to approximations of undetermined accuracy.

Stress analysis of notched laminates may help to understand and predict the onset of damage in the form of matrix cracks and delamination. However, the damage causes redistribution of the stresses in the laminate making the stress analysis of the undamaged laminate of little value in predicting strength [9]. Static strength models for notched laminates have been developed that do not require a stress analysis of the damaged laminate. Instead, the strength of the notched and the unnotched laminates are compared. In 1974 Whitney and Nuismer [10] suggested a failure criterion that predicts the uniaxial tensile strength and is based on a simple consideration of the isotropic stress distribution rather than on the actual state of laminate stresses. Their failure criterion features two versions: the first one predicts failure if the material is critically stressed over a certain distance from the hole; the second one predicts that

a laminate will fail if the average stress over some other distance away from the hole exceeds a certain value.

However; their models determine the ratio of the notched strength to the unnotched strength of a laminate so that the latter must be known; moreover, they are dealing with the different mechanisms of straight edge driven versus notch initiated failure simply by adjusting the material dependent parameters. After collecting data for both unnotched and notched laminates, failure loads for various notch sizes can be predicted.

Three years later Whitney and Kim [11] published the results of a test series which exhibit that notched failure mechanisms differ from those in the unnotched situation. They investigated the influence of laminates with two different stacking sequences, one of them producing tensile, the other producing compressive, interlaminar normal stress througout the thickness of the straight edge on both notched and unnotched specimens.

The data indicate that unnotched tensile strength is reduced by tensile interlaminar stresses along the straight edge and is strongly dependent on the stacking sequence; while the strength of notched specimens is independent of the straight edge effects since tensile failure is initiated by the locally high stress at the notch before straight edge

delamination comes into effect. Other investigations of the fatigue behaviour of notched specimens were conducted by Sendeckyj [3], Stinchcomb and co-workers [2], and Whitcomb [9]. The work most comparable to the present one is that of Whitcomb, who described the damage state and the mechanical response of four different notched laminates after fatigue loading and related delamination onset to the results of a FEM stress analysis. The load levels of two-thirds of the initial strength of the laminates correspond to fatigue lives greater than ten million cycles. At this point, the damaged specimens were investigated using destructive and nondestructive methods. The residual strength of all laminates was equal to or higher than the initial strength of the specimens. Stiffness degradations were found to be in the range from zero to 10 percent. Whitcomb also presented figures comparing initial stress distributions with delaminations at different locations through the thickness on the hole edge that suggest that interlaminar normal stress and shear stress distributions govern the locations of first fatigue delaminations. Later in the lifetime, the direction of delamination growth can be changed by an altered stress distribution.

Sendeckyj's work is mainly concerned with the introduction of stereo X-ray radiography and describes the damage

that is made visible on X-ray stereo pairs. The emphasis of the paper of Stinchcomb and co-workers is on the investigation of constraint effects on the development of initial damage. Notches were introduced in specimens by cutting notches out of single plies before lamination. The surface plies of the laminates to be produced were left undamaged. The results of their work can be partially related to damage-pattern characteristics found in the present work which are dependent on the stacking sequence.

In the first phase of the present study, the fatigue damage pattern was observed in laminates with four different stacking sequences. For further investigations, two of the laminates with relatively little straight edge initiated damage were chosen in order to isolate notch related damage from straight edge driven damage as much as possible.

The damage induced by static and by fatigue loading was observed by nondestructive inspection and other methods. Cyclic and monotonic tests were performed to compare the development of damage under cyclic loading with that under static loading. Residual tensile strength tests were conducted on damaged specimens to determine the relationship between loading history, damage state, and strength.

II

2.0 EXPERIMENTAL PROCEDURES

2.1 MATERIAL AND SPECIMENS

The material used in this study was T300-5208 graphite epoxy. The specimens for the preliminary study were ten inches long, 1.5 inches wide and had a 0.25 inch diameter hole in the center. The four stacking sequences were:

$$[\ 0,+45,-45,\ 90]_s$$
$$[\ 0,\ 90,+45,-45]_s$$
$$[\ 45,\ \ 0,-45,\ 90]_s$$
$$[+45,-45,\ \ 0,\ 90]_s$$

From the results of mechanical and nondestructive tests on these laminates, two stacking sequences were chosen for further investigation of notch related damage. They were:

$$[\ 0,\ 90,+45,-45]_s \qquad \text{type A}$$
$$[+45,\ 90,-45,\ \ 0]_s \qquad \text{type B.}$$

The new specimens had a 0.375 inch diameter center hole machined using an ultrasonic drilling machine. A third stacking sequence,

$$[+45,-45,0,90]_S \qquad \text{type C}$$

was used to determine the critical strain energy release rate for delaminations in the batch of material used for this study. These specimens had no hole.

2.2 MECHANICAL TESTS

All mechanical tests were conducted in load control on a 20 kip servo hydraulic, closed loop MTS testing machine.

Mechanical tests were performed to obtain strength and stiffness data for the undamaged and damaged specimens and to impose cyclic loading histories on the specimens.

The test machine was equipped with MTS hydraulic grips. The ends of the specimens seated in the grips were wrapped with a double layer of sandpaper folded around the upper and the lower edge such that the vertical edges of the specimens remained uncovered. This is merely a precaution to avoid slipping of the grips under high tensile loading. The sandpaper should be replaced regularly. Alignment plates fill-

ing in the gaps between the specimen edges and the inner surface of the grip housing helped to align and position the specimen and thereby reduce unintentional load components like bending moments. Correcting a relative twist between the upper and the lower grip avoided unintentional twisting moments acting on the specimens. Any relative twist was minimized by placing alignment bars between the grips and rotating the lower grip until the pointer and the crossmark on the alignment bars matched. The specimen, equipped with sandpaper and the alignment plates, was placed in the lower grip, and the gripping pressure was adjusted so that the specimen was still moveable against friction. Then the lower grip and specimen were moved up by hydraulic pressure until the upper part of the specimen and the alignment plates were in the right position within the upper grips. While the control set point was adjusted such that the lower grip was moving down at a very low time rate, both grips were slowly tightened. This procedure guarantees an almost buckle free positioning of the specimen under a slight tensile load. However; it was necessary to clean the grip housing and the wedges periodically because dirt on their contacting surfaces can cause unintentional relative twists of the wedges while tightening.

2.3 MONOTONIC LOADING TESTS

The specimens were loaded at time rates between 25 lbs/sec and 50 lbs/sec using the ramp function of the MTS function generator.

Each of the four laminates used in the preliminary study was loaded until failure occurred in order to obtain the stiffnesses and strengths of these laminates.

Strain was measured by a 1.0 inch extensometer attached by rubber bands to the specimen. Slipping of the extensometer was prevented by pressing the knife edges into strips of double adhesive tape attached to the specimens. The extensometer was centered with respect to the notch and oriented for measuring the longitudinal strain only.

Stiffness curves were recorded on an X-Y plotter. Some tests were performed on damaged specimens to obtain changes of stiffness and strength dependent on the loading history.

Five specimens of each of the new laminate types A, B and C were subjected to strength tests with stiffness and acoustic emission recording to obtain the tensile strength, initial stiffness and information on damage events during the loading process. Monotonic tests were also performed on damaged specimens to measure the effects of cycling loading on strength and stiffness. Stiffness was measured during several tests with a 1.0 inch extensometer and a 3.625 inch

extensometer to obtain information on the strain values around the hole based on short and long gauge length.

2.4 SEQUENTIAL LOADING TESTS

Valuable information about a typical fatigue effected damage state distinguished from a damage state caused by monotonic loads was obtained from sequential loading tests. Two specimens, A22 and B16, were loaded in tension to a low load, treated with zinc iodide (a medium nearly opaque to X-rays) unloaded, X-rayed, and loaded again to a greater load. This procedure was repeated until failure. For each loading procedure, a stress-strain curve was recorded. The specimens were instrumented with the 3.625 inch extensometer. Beginning at a very low load level, the specimens were sequentially loaded in increments of 10 percent of the mean tensile strength until a stress equal to the tensile strength of the virgin specimens was reached. Then the increment was lowered to 5 percent of the tensile strength and the sequential loading was continued until the specimen failed.

2.5 FATIGUE TESTS

All fatigue tests were run in the tension-tension mode with a load ratio of R=0.1 and a frequency of 10 Hertz.

Specimens were tested at several different load levels designated as percentages of the mean tensile strength of five samples. The load levels spanned the range from 70 to 95 percent; i.e. from long-life-load levels to short-life-load levels.

Several specimens were run to failure to obtain S-N curves, others were monotonically loaded to failure after a certain number of cycles to obtain the strength-versus-loading-history curves. Many of these specimens were subjected to nondestructive inspections such as X-ray radiography or moire tests at selected numbers of cycles.

Continuous stiffness degradation curves were produced using a Z-80 microprocessor and a peak-detector program. The inputs for the microprocessor were load and strain signals from the MTS load cell and strain amplifier, respectively. The microprocessor evaluated the average load range and strain range during a time period of one second (10 cycles). These data were used as the input for a peak detector program. The initial load and strain range data were used to define an initial stiffness value based on the unnotched cross-sectional area. All subsequent stiffness

data were referred to as percentages of the initial stiffness. Results were printed at each 0.5 percent stiffness loss. Additionally the continuously updated stiffness-cycles curve was displayed on the terminal screen and could be plotted on paper. The printed results were used to produce stiffness degradation plots on both real and logarithmic lifetime scales. However, it was not possible to record the values of stiffness degradation during approximately the first 100 cycles since the peak detector program is not started until the desired loading conditions are imposed on the specimen.

2.6 X-RAY RADIOGRAPHY

The X-ray photographs were taken using a Hewlett Packard N Faxitron X-ray system, using the voltage of 25 Kv for all exposures.

The specimens were held by a device which allowed the specimens to be tilted from zero to about 45 deg with respect to the horizontal plane. The distance of the film from the beam source was about 18 inches.

Stereoscopic investigation is possible by taking two radiographs of the same specimen, each at a different angular position with respect to the direction of the X-ray beam. For the stereo negatives Kodak-R-film was exposed for

0.6 minutes. If a 3-D investigation was not intended, Kodak M-film was exposed for 0.3 minutes.

To make damage, especially matrix cracks but also delaminations, visible on X-ray photographs, the specimen must be prepared by filling the openings of the damage zone with a contrast medium. In the present study the specimens were moisturized at the edges of the hole and at the straight edges with zinc iodide which is nearly opaque to X-rays. The zinc iodide was applied shortly before the end of a cyclic test so that the relative movement of material adjacent to cracks helped it penetrate into the damage zone; however, the time of cyclic loading with contrast medium in the specimen was kept short to avoid effects of zinc iodide on the fatigue behavior. For monotonic test conditions, the zinc iodide was allowed to soak in under load for some minutes. Load levels for the purpose of letting the contrast medium penetrate were the maximum load applied during the test or a somewhat lower load in cases where the testing load approached or exceeded the tensile strength of a specimen.

The excess zinc iodide on the surface had to be washed out carefully using acetone in order to avoid concealing the damage pattern by the image of the surface. Although this method of detecting damage within a specimen gives highly precise information about the location and the size of even

single matrix cracks, it must be critically mentioned that only those cracks which are penetrated by the contrast medium are visible; on the other hand, the zinc iodide can only penetrate along cracks which are connected with a surface. Therefore, those cracks which are not connected with the surface where the zinc iodide was applied can not be made visible on X-ray photographs. There is, however, an advantage in this weakness: applying the contrast medium only at the edge of the hole gives good information on what part of the damage initiates there. Similar observation can be made for the damage associated with the straight edges. Using the moire test device, specimens could be loaded during X-ray exposure; however, only few photographs of loaded specimens could be taken.

In agreement with Sendeckyj's observations [3], delaminations appear as dark regions with diffuse edges and sometimes have lighter areas embedded which are sharply distinguished from the surrounding spot. As in the present study, the light areas usually appear on X-rays of highly damaged specimens. It is believed that the variations in darkness are formed by mechanisms illustrated in Figure 1.

At the periphere of a delaminated area, the gap between the delaminated plies is small, offering space for only a thin layer of penetrant that slightly reduces the intensity

Penetrant Distribution

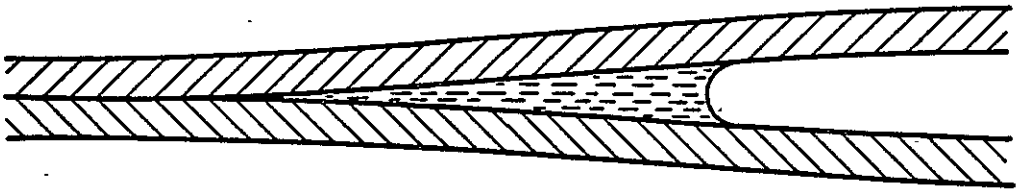

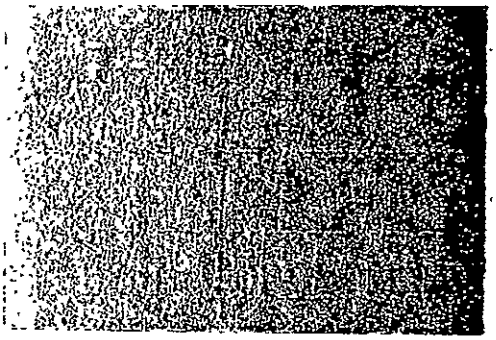

Effect on X-Ray Photograph

Figure 1: Penetrant Distribution in a Delaminated Area

of passing X-ray beams and leads to the effect of diffuse edges. With increasing distance from the periphere, the thickness of the penetrant layer increases up to the point where the bond between the fluid and the solid material is no longer sufficient to form an uninterrupted layer. This transition phase is small and gives the distinct limits of the light spots. Thus, the light areas indicate a minimum gap width between delaminated plies.

2.7 DEPLY TECHNIQUE

The deply technique gives information on the location and extent of delaminations and fiber cracks. The specimens were kept at a temperature of 785 deg Fahrenheit for 30 to 50 min. in an electrically heated oven with controlled air exchange. This process effects the destruction of the resin-rich layer between the fiber carrying plies (the ply interface), which could then be separated and filed on paper cards for investigations such as photography or microscopy. Applying gold chloride solution to specimens before the heat treatment helps identify regions of delaminations and fiber cracking. Layers to be deplied were first fixed by applying sticky tape and then disconnected from the remaining laminate by using a knife edge to systematically enlarge already present gaps.

As a general result of the experimental part of this study, the interlaminar surface patterns of deplied specimens consist of four elements. A surface showing exposed fibers looks typically silky or shiny and covers the largest part of the area. The ply surface contains evenly distributed spots of residual resin that are oriented in the fiber direction of the adjacent layer of the intact laminate. More significant for damage studies are the spots colored by gold chloride and characteristic dark blue areas. These are often accompanied by a concentration of resin-rest spots and match the locations of the previously mentioned dark areas on X-ray photos. It is believed that the blue color arises from zinc iodide since the deplied specimen underwent X-ray radiography before deplying. However, the contrast on the deplied surfaces was so poor that, instead of a photographic documentation, sketches of the damaged zone were drawn.

2.8 MOIRE TECHNIQUE

2.8.1 Purposes

The moire technique can be used as an accurate tool to obtain the complete two-dimensional displacement field on the plane surface of loaded elastic bodies. Because of its accuracy it is widely used to experimentally obtain elasticity solutions that cannot be determined analytically or to

judge the validity of approximate solutions. Another important feature of the technique is its ability to show the effects of structural damage within a body on its elastic behavior. In other words, using the moire technique, it is possible to obtain the stiffness changes in damage zones.

2.8.2 Theoretical Background

Mechanical interference or coarse moire produces the same fringe pattern as moire interferometry. Here the test setup consists simply of two coarse gratings with frequencies between 1 line/mm and 40 lines/mm. One is fixed in space and is called the reference grating; the other undergoes in-plane deformations and is called an active grating. In practice, the active grating is attached to a body whose deformations under certain loading conditions—are to be measured.

If for instance the active grating is uniformly stretched, a fringe pattern of equidistant light and dark zones appears. Any of these fringes is the location of equal displacements of points on the active grating. The moire fringe orders N_x and N_y are the number of subsequent changes of intensity experienced at a certain point during the loading process from zero to the final value. The corresponding displacements u and v can be calculated by:

$$u = gN_x$$

$$v = gN_y \tag{2.1}$$

where g is the pitch of the reference grating.

The same principle of using a fringe pattern to measure in-plane displacements is used for moire interferometry, which uses much finer gratings with pitches on the order of magnitude of the wavelength of light and therefore involves the effects of diffraction and interference of light.

Figure 2 illustrates the principle of a transmissive moire test setup as it can be used in practice for an investigation of the elastic behavior of a transparent body. In Figure 2a the beam of coherent parallel directed light is diffracted at the reference grating into only two symmetrically oriented beams of diffraction order 0 and 1. The conditions for this arrangement can be calculated using the grating equation:

$$\sin\theta_m = m\lambda f + \sin\alpha \tag{2.2}$$

and implementing the condition of symmetry of the diffraction orders 0 and 1.

$$\sin\alpha = \frac{\lambda}{2} f \tag{2.3}$$

with

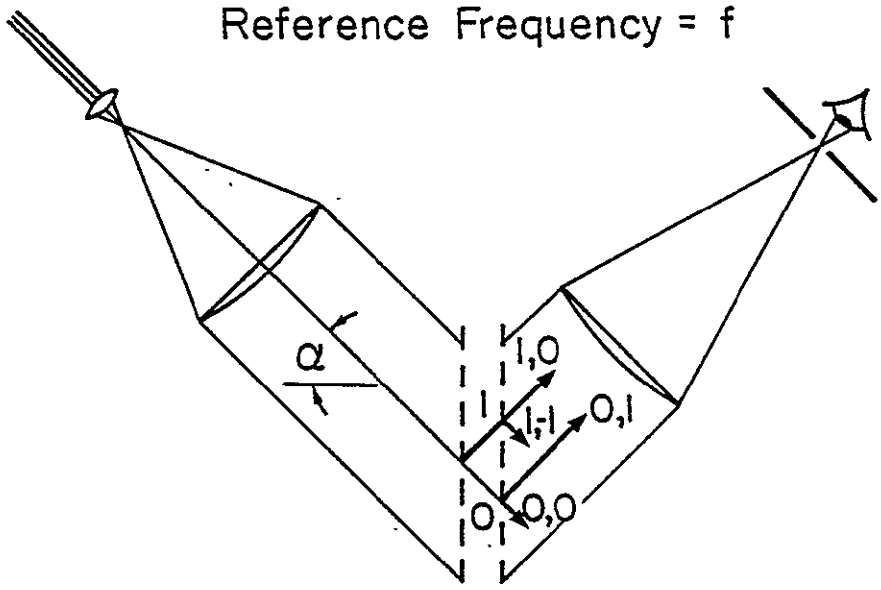

a) Active Frequency = $\frac{f}{1+\epsilon}$

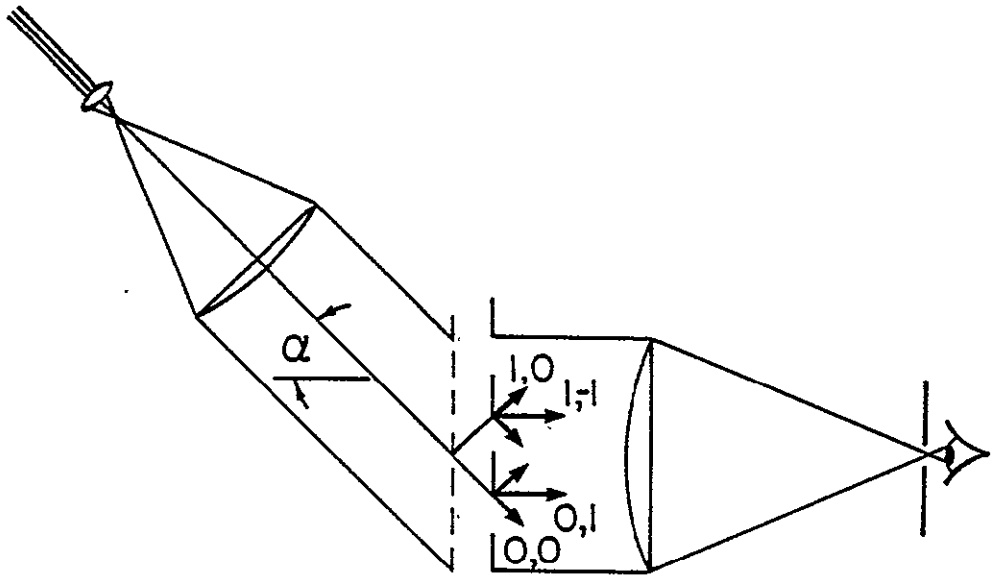

b) Active Frequency = $\frac{f}{2(1+\epsilon)}$

Figure 2: Transmissive Moire Test Set Up

α = angle of incidence

θ_m = direction of the diffracted light

m = diffraction order, counted counter clockwise

λ = wavelength of the coherent light

f = frequency of the optical grating

Two, and only two, diffraction order are produced if

$$\frac{2}{\lambda} > f > \frac{2}{3\lambda} \tag{2.4}$$

The beams of the diffracted light are diffracted again at the active grating. Since the strain is zero, both grating frequencies are equal and the beams of the diffraction order 1,0 and 0,1 are parallel, thus having parallel wavefronts.

If the active grating is deformed, however, the angles of the beams of diffraction order 1,0 and 0,1 are different according to the grating equation. The angle orientations of their wavefronts differ by the same value and produce a fringe pattern in space as is depicted in Figure 3.

An important improvement of this setup is to choose an active grating with an undeformed frequency being one-half the value of the reference grating so the beams of the order 1,-1 and 0,1 emerge perpendicularly from the plane and allow an unforeshortened view of the fringe pattern, Figure 2b.

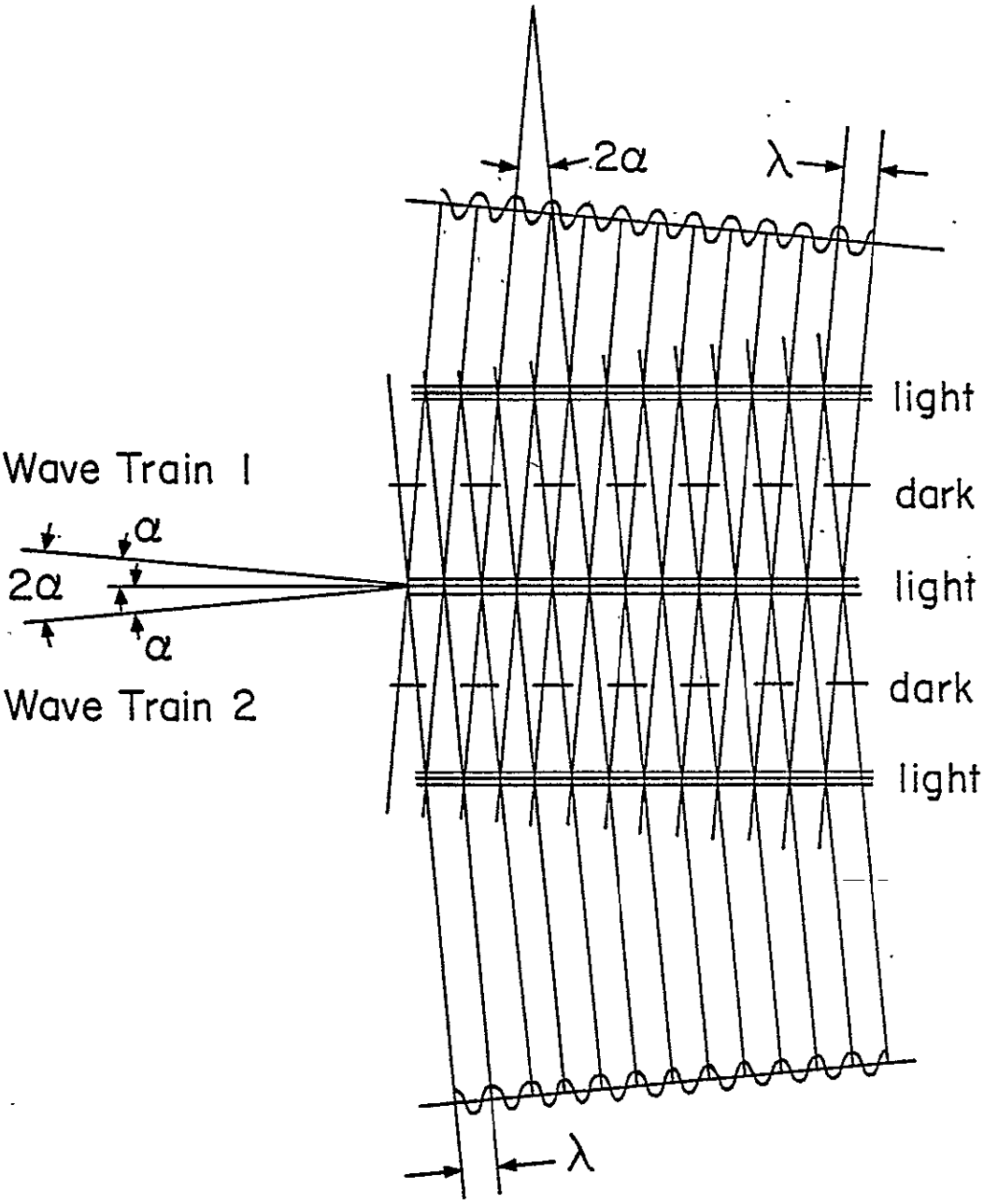

Figure 3: Interference of Two Wavefronts of Coherent Light

Another effect of decreasing the pitch of the reference grating by even multiples is called moire fringe multiplication. For a given active grating frequency there are β times as many fringes produced if the reference grating frequency is β times higher than the active grating frequency.

Another modification is inevitable if the body to be investigated is opaque. Without changing the theory or the resulting fringe pattern the transparent active grating is replaced by a reflecting grating, and the effect of the reference grating has to be achieved by a so called virtual grating. A virtual grating produces two beams of coherent light just as the reference grating did, as is illustrated in Figure 4.

2.8.3 Loading Fixture

The size of the graphite epoxy specimens required the construction of a new loading fixture for making moire measurements under load. The design, although kept as simple as possible, allows stresses as great as the tensile strength of the specimens to be applied. At the same time the creation of any out-of-plane effects is eliminated by making all forces colinear. The actual applied load can be measured through strain gages attached to a calibrated bolt, which is designed for undergoing suitable strains within the load levels in question.

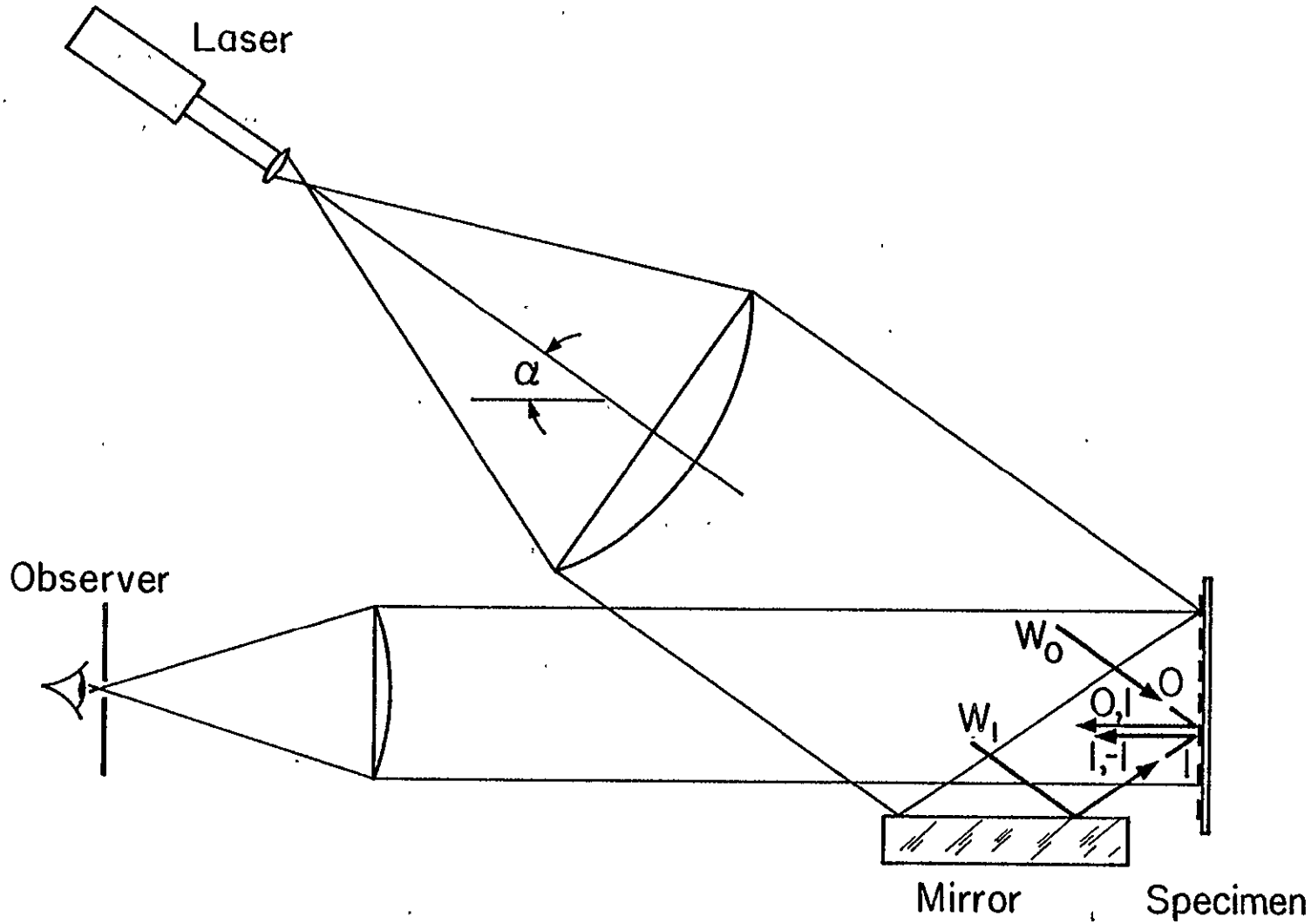

Figure 4: Reflective Moire Test Set Up with Virtual Grating

For the moire test, the device is being attached to a vertical surface and held by only one screw whose axis passes through the hole in the specimen. This allows the device to be turned around the axis to obtain displacement fields in both the X-direction and the Y-direction of the laminate. The device consists of the frame, the carriage, the load cell, the torsion eliminator, the back plate, and two holders, Figure 5. The frame contains the lower grip for the specimen and guides the movable carriage and the torsion eliminator. The back plate is fixed to the end of the frame and holds the loading screw. The force, applied by turning the screw, is transmitted on the specimen through the torsion eliminator, the load cell, and the carriage. The torsion eliminator interrupts the transmission of the torsional moment from the screw on the load cell. For simplicity, the load is transmitted on the specimens not by friction but mainly through two pins in the center of each grip. The specimen ends are reinforced by glass epoxy laminates. All parts are dimensioned such that the forces in them have the same centerline, thus avoiding bending moments and other out-of-plane effects. As a result, the load cell, consisting of a steel rod with threads and attached strain gauges is free of torsional and bending moments. The four strain gauges are attached such that the first two measure the

positive longitudinal strain on each side of the rod, giving a positive signal, while the second two measures the negative transverse strain (Poisson strain) on each side, also giving a positive signal. The sensitivity of the device is thereby increased by the factor $2(1+\nu)$ (ν is Poisson's Ratio), while at the same time the effect of thermal expansion is eliminated. The load measuring device was calibrated by using an Instron-test machine. The applied loads were measured and plotted against the corresponding strain recorded by the load cell.

2.8.4 Preparation of Specimens for Moire Tests

During a moire test the load is transmitted to the specimen through the pin and the edge of the holes drilled at the ends of each specimen. Since the magnitude of the load may come close to the static strength of specimens the ends were reinforced to prevent their breakage. The reinforcements consist of $[0, 45, -45]_s$ glass-epoxy plates which are glued to both sides of each specimen, using a two-component epoxy adhesive.

To produce high quality moire fringe patterns, the specimen plane, with the grating, and the surface planes of the reinforced ends must be parallel. If those surfaces are not parallel to each other, bending will be introduced during a

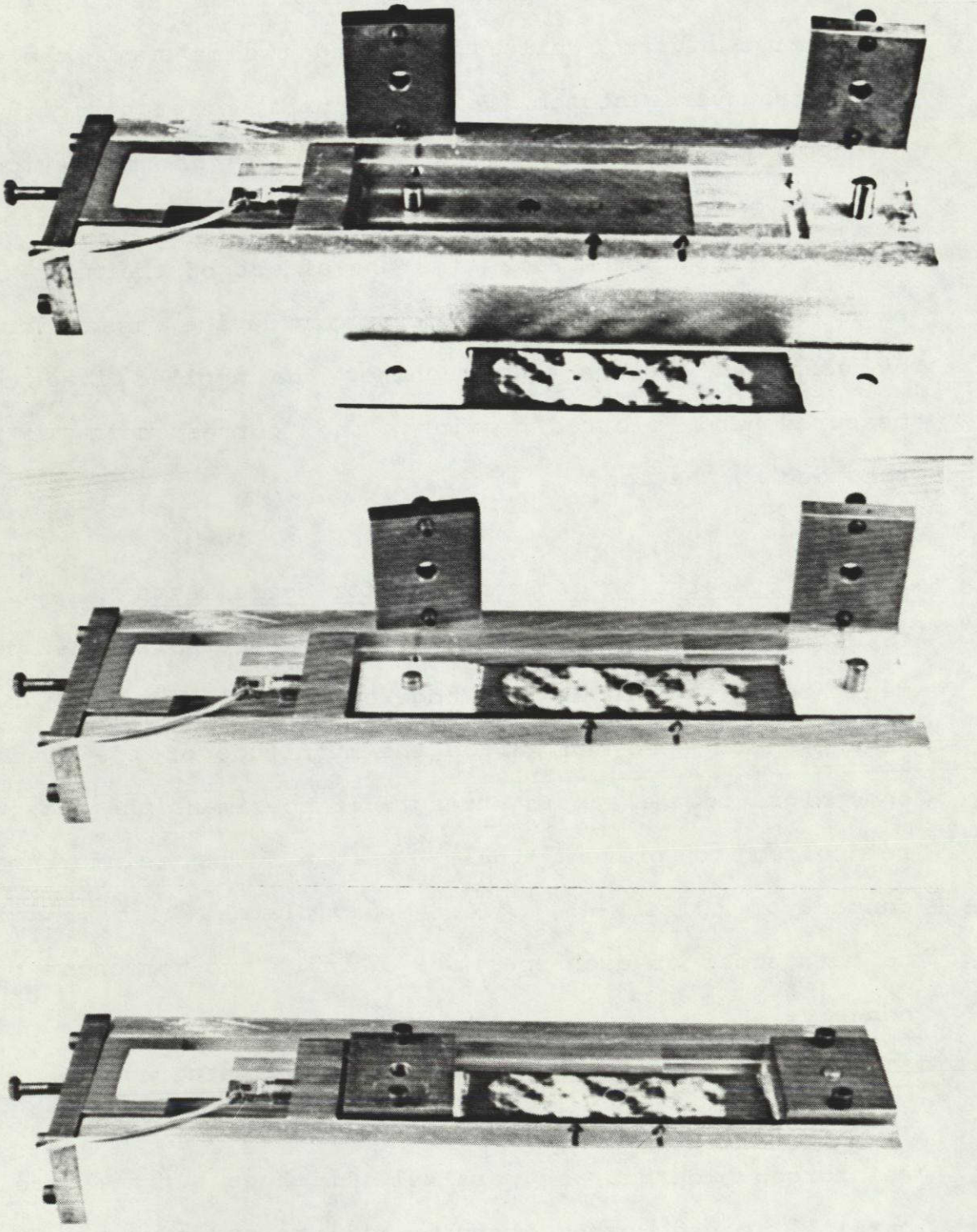

Figure 5: Loading Fixture

test and the result will be falsified. All surfaces to be glued together were sanded and cleaned with acetone. A thin layer of adhesive was spread onto the prepared surfaces, then the pieces were put together so that the reinforcement plates were attached to one side of the specimen at a time. The specimen was then placed on a thick glass plate, another plate was set on the middle of the specimen, and a heavy weight with a plane surface was set on top of the specimen, thus improving the adhesive bond and ensuring the parallelism of reinforcement plates and specimen surfaces. The plate on the middle of the specimen helped eliminate bending during the curing time of the epoxy.

The holes in the tabs were machined to provide a press fit with the loading pins to achieve a symmetric distribution of pressure at the edge of the holes.

During the specimen fabrication process, the pattern of the curing cloth was formed in the matrix material on the specimen surface. To provide a surface that is plane and smooth enough to support an optical grating two different approaches can be taken. The first method is to polish the surface down until the curing cloth pattern is removed and a smooth surface is left. This method has two disadvantages. The first one is that some of the pattern might remain while, at the same time, the outside layer of fibers is

exposed. Damaged fibers on the surface of the specimen reduce the adhesibility of the grating, may cause local distortion of the displacement fields, and may reduce strength. The other disadvantage is that removing of matrix material from the surface disturbs the balance of residual stresses within the laminate, thus leading to its bending in the unloaded state. This has probably only little effect on the specimen behavior during moire tests but makes proper attachment of the grating more difficult.

In the second method, the holes of the surface pattern are filled with epoxy material rather then removing the embossed parts. For this purpose epoxy adhesive is spread onto the surface and then covered by a teflon strip under firm pressure. Shrinkage of the hardening epoxy then leads to a less coarse reproduction of the original pattern rather than to its complete removal.

Therefore, a combination of the two methods seems to be recommendable. Instead of polishing down the whole pattern, fine sandpaper was used to remove the coarsest uneven patches only. The epoxy adhesive method was then applied. This avoids disturbing the balance of residual stresses while at the same time the surface is fine enough to apply the epoxy technique successfully.

The optical grating was produced by exposing a photographic plate to two interferential beams of coherent light. After developing, the photo layer bears a pattern of equidistant bars and furrows. The furrows are at locations where the light sensitivity was lower and the remaining unreacted silver particles were washed out to a higher extend. The surface of the photolayer was then treated with photoflo, what lessens the adhesibility to the coating to be attached later. Using a vacuum chamber in order to minimize oxygeneous reactions, an aluminum layer was produced by evaporating this metal using electrically heated wire. The photographic plate was later glued to the prepared surface of the specimens. After hardening of the glue, the glass plate bearing the photographic layer was removed and the very thin metal foil with the imprinted negative image of the grating was left; thus, the specimen was ready for the moire test.

2.8.5 Test Matrix

Moire tests were run for an A-specimen and a B-specimen at logarithmically distributed stages of lifetime from 10^0 to 10^5 cycles or to $6x10^5$ cycles. Fringe patterns of the displacement fields in both the x- and the y-directions were recorded. The specimens were tested under loads varying from a nominal load of 50 lbs to a load of 1550 lbs, which is about 60 percent of the static strength.

For stiffness measurements, the effect of frequency mismatch is eliminated if there are two fringe patterns under different loads available. In this case, the difference in fringe order and the load increment can be used to obtain a correct stiffness value. It also must be determined if the actual reference frequency is lower or higher than the theoretically desired one. In the latter case, the null-field-fringe order must be counted negative in order to obtain a proper correction.

III

3.0 DISCUSSION OF TEST DATA

3.1 X-RAY PHOTOGRAPHY

During the following discussion cracks that are initiated at the hole boundary or the straight edge will be called primary cracks. Other, usually smaller cracks, which initiate along the primary cracks are located in adjacent plies and will be called secondary cracks. For locating the angular position of damage around the hole, a reference axis, coincident with the loading direction and the direction of zero deg plies, is defined. Positive angles (θ) are measured counter- clockwise from the reference axis.

3.1.1 A-Specimens

3.1.1.1 Quasistatic Damage Patterns

The radiographs of quasistatic tests with repeated and increasing load applications give some data about the initiation of damage.

The first visible cracks for specimen A-22 appear at 60 percent of the average initial strength for A-laminates, Figure 6a. They are zero-deg cracks on both sides of the hole, having equal extensions in both directions, and shorter, 90-deg cracks also on both sides of the hole,

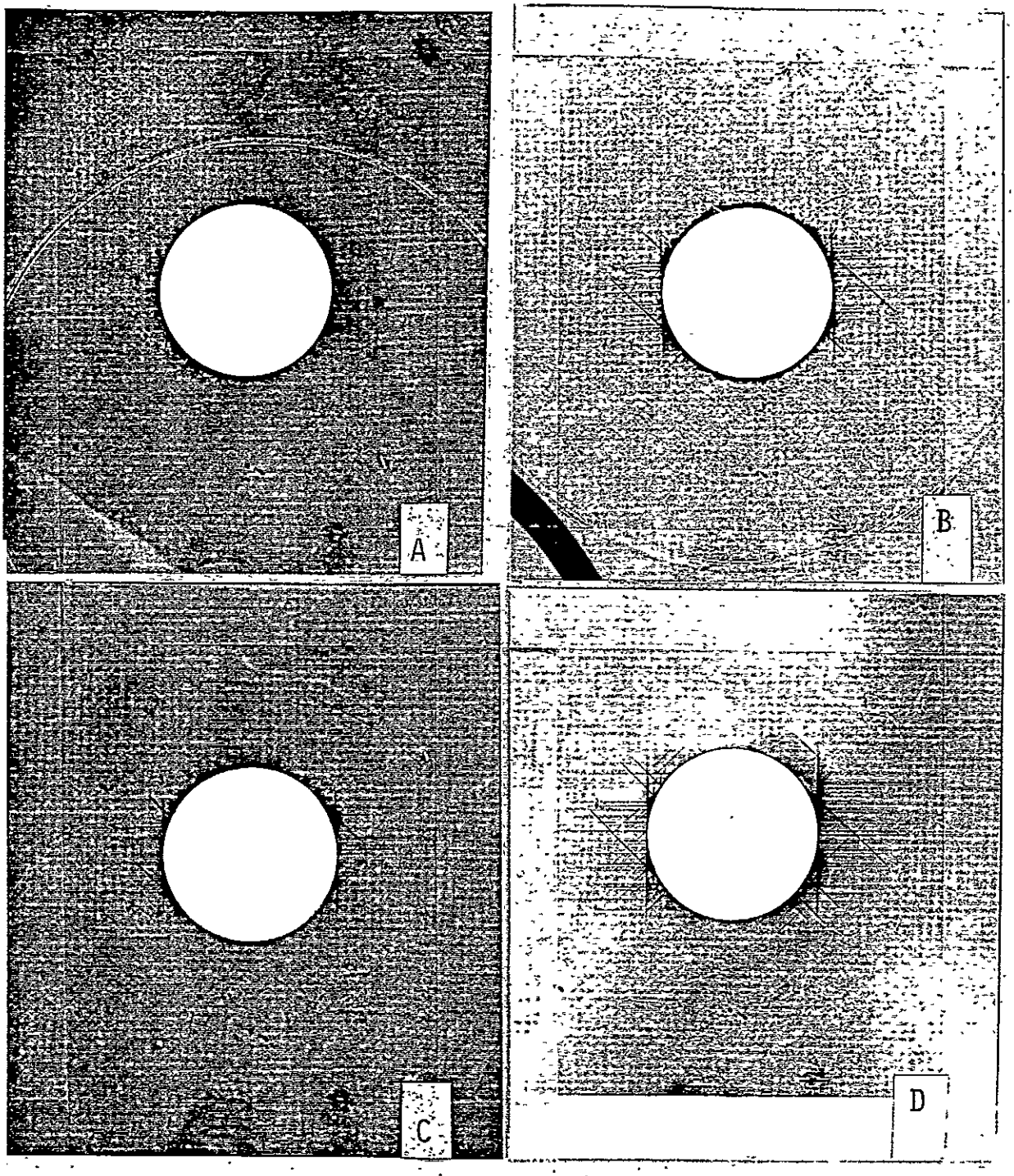

Figure 6: Quasi-Static Damage in an A-Laminate

extending along the 90-deg direction less than one-fifth of the hole diameter. This very early pattern of damage in zero-deg and 90-deg plies is completed by matrix cracks in the 45-deg plies.

The 70 percent radiograph of the same specimen shows very well defined +45-deg cracks along a line passing through the center of the hole. The cracks tangent to the hole are much smaller. Very small secondary -45-deg cracks develop along the other cracks, Figure 6b.

In the radiographs following the 80 percent and 90 percent steps, the tangent zero-deg cracks appear darker but do not increase in length very much. The density and then the length of the 90-deg cracks, still confined to the area governed by the zero-deg cracks, increase considerably. The +45-deg cracks tangent to the hole grow rapidly into the area which is already occupied by the 90-deg cracks.

The first delaminations were stereo-optically detected in the 90/45 interface after loading to the 80 percent level and are more clearly observed in the radiograph made after the 90 percent load level. Figures 6c and 6d show the initial delaminations bounded by matrix cracks and the edge of the hole in the regions $\theta \simeq 60$-deg and $\theta \simeq 120$-deg.

The highest load levels are characterized by a greater number and increased length of -45-deg cracks and by a

butterfly pattern of delamination around the hole. The observations suggest that the onset of delamination is at least assisted by, if not caused by, the existing matrix crack pattern.

3.1.1.2 Fatigue Damage Patterns

The damage patterns discussed in this section belong to several type A specimens which were subjected to different numbers of cycles at the 80-percent load level. The X-radiograph of A-14, Figure 7a, shows damage after 10 cycles at the 80 percent load that is very similar to that shown in Figure 6c. A low penetration with zinc iodide is the probable cause for the 90 deg cracks not showing up clearly in this figure. The matrix crack pattern after 1K cycles shown in Figure 7b shows an increase in length of all cracks. Additionally, the specimen developed delaminations at the edge of the hole $\theta \approx 135$ deg and $\theta \approx -45$ deg. After 10K cycles these delaminations are more developed and new delaminations in the $\theta \approx 45$ deg and $\theta \approx -135$ deg regions are initiated. The zero-deg tangent cracks now extend beyond the area of the hole while cracks in the other plies are also longer. The damage in specimen A-4 with 10K cycles of fatigue loading, Figure 7c, prevents a generalization of the delamination development shown in the previous photographs.

Namely, the delaminations at the -45/135-deg locations are less developed than in A-4. The delaminations are now following the path of the tangent cracks which are 40 percent longer than the hole diameter. Cracks in the 45-deg direction are longer than those in the -45-deg direction. A large number of 90-deg cracks have developed; many of them initiate at the tangent zero-deg cracks, and some approach the straight edge.

The damage state after 100K cycles in A-39 is shown in Figure 7d. The zero-deg cracks have an extension of 190 percent of the hole diameter and are still accompanied by delaminations, mostly on the side facing the straight edge. Delaminations also developed along the hole edge between the tangent cracks.

Figure 8 shows a highly developed damage state after 600K cycles in specimen A-39. Other specimens cycled at the 80-percent load level survived 900K to 1300K cycles. The damage zone includes large delaminations of an obviously complex distribution and the tangent zero-deg matrix cracks passing through it, matching its extension. New zero-deg cracks of a large size have formed in the middle between the tangent cracks, and one is seen between the hole and the straight edge. The +45-deg and the 90-deg cracks extend from the edge of the hole to the straight edges. Some

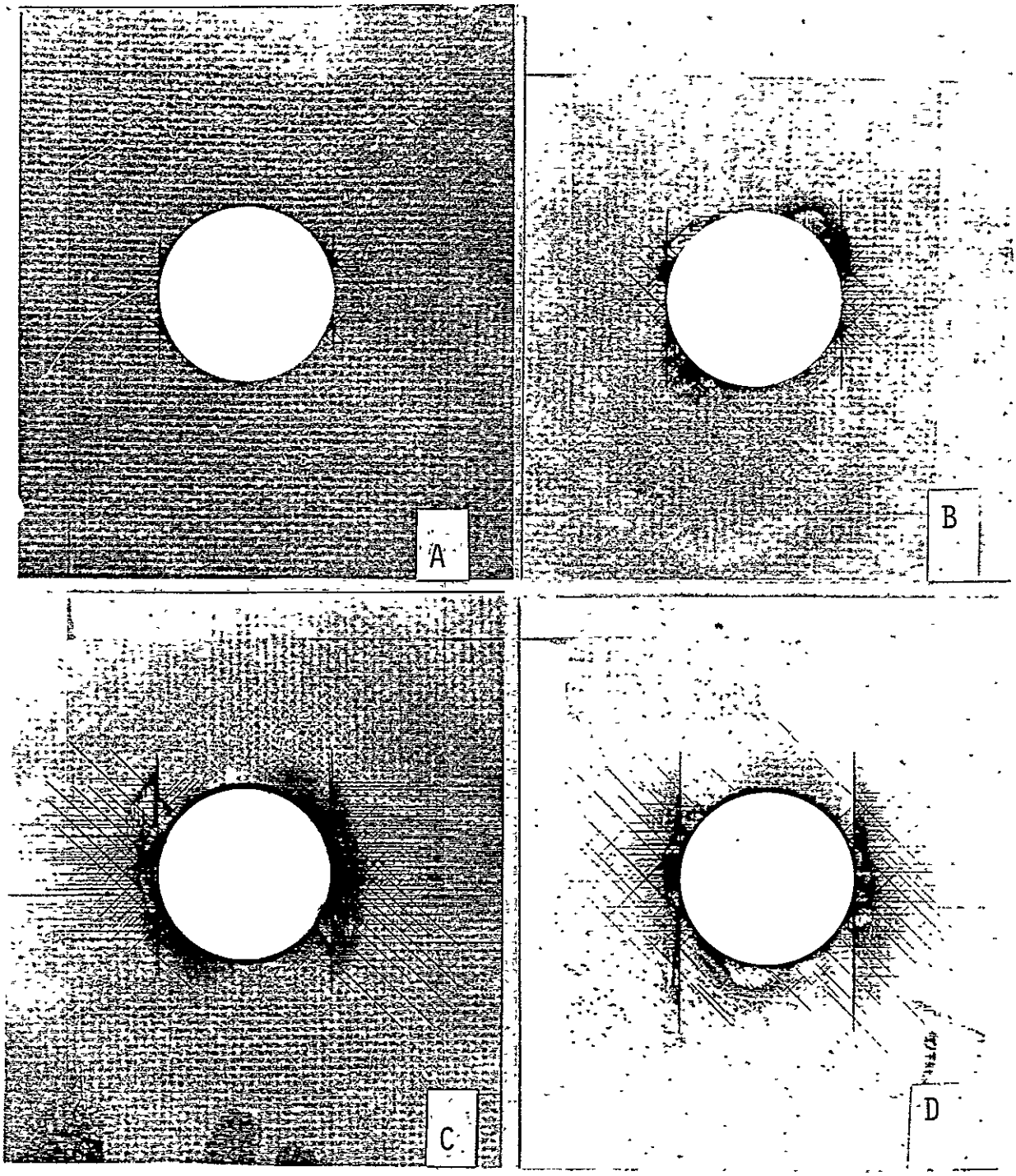

Figure 7: Fatigue Damage in an A-Laminate

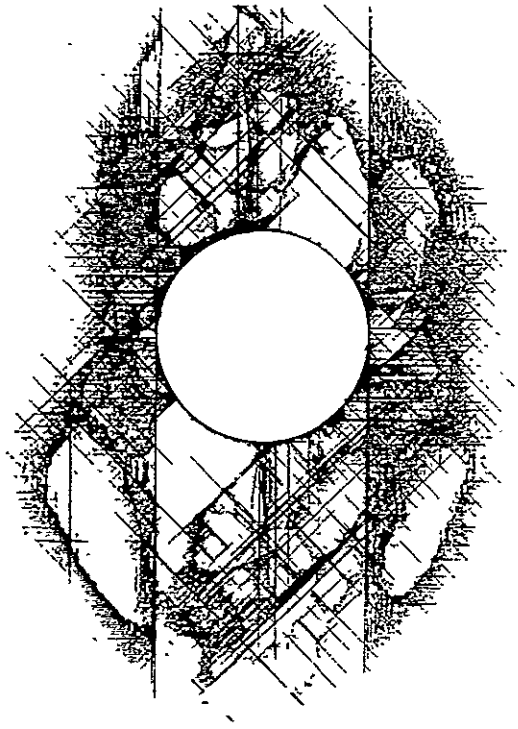

Figure 8: A-39 after 600K Cycles at 80 Percent Load Level

matrix cracks and a delamination initiate on the straight edge.

It is mentioned here that this specimen at this stage of fatigue loading had a residual strength of 122 percent of themean strength of undamaged specimens, and the 1.0-inch extensometer measured a stiffness of approximately 65 percent of the mean stiffness of undamaged specimens.

3.1.2 B-Specimens

3.1.2.1 Quasi-static Damage Pattern

The radiographs taken during the quasi-static test on specimen B-16 show the first matrix cracks in the +45-deg plies on lines which pass through or near the center of the hole at the 50 percent load level, Fig. 9a. The next picture, Fig. 9b, taken after application of a 60 percent load, shows cracks in all plies. While the previous cracks grew only a small amount, new cracks in the +45-deg direction are added. These follow lines that pass through the hole but closer to the periphery than to the center, and extend away from the boundary of the hole. The new cracks in the +45-deg direction have the same size as the initial ones. Cracks in the zero-deg plies initiate tangent to the hole and extend into the region containing cracks in the +45-deg plies. Along the new +45-deg cracks, equidistantly distributed small, 90-deg cracks

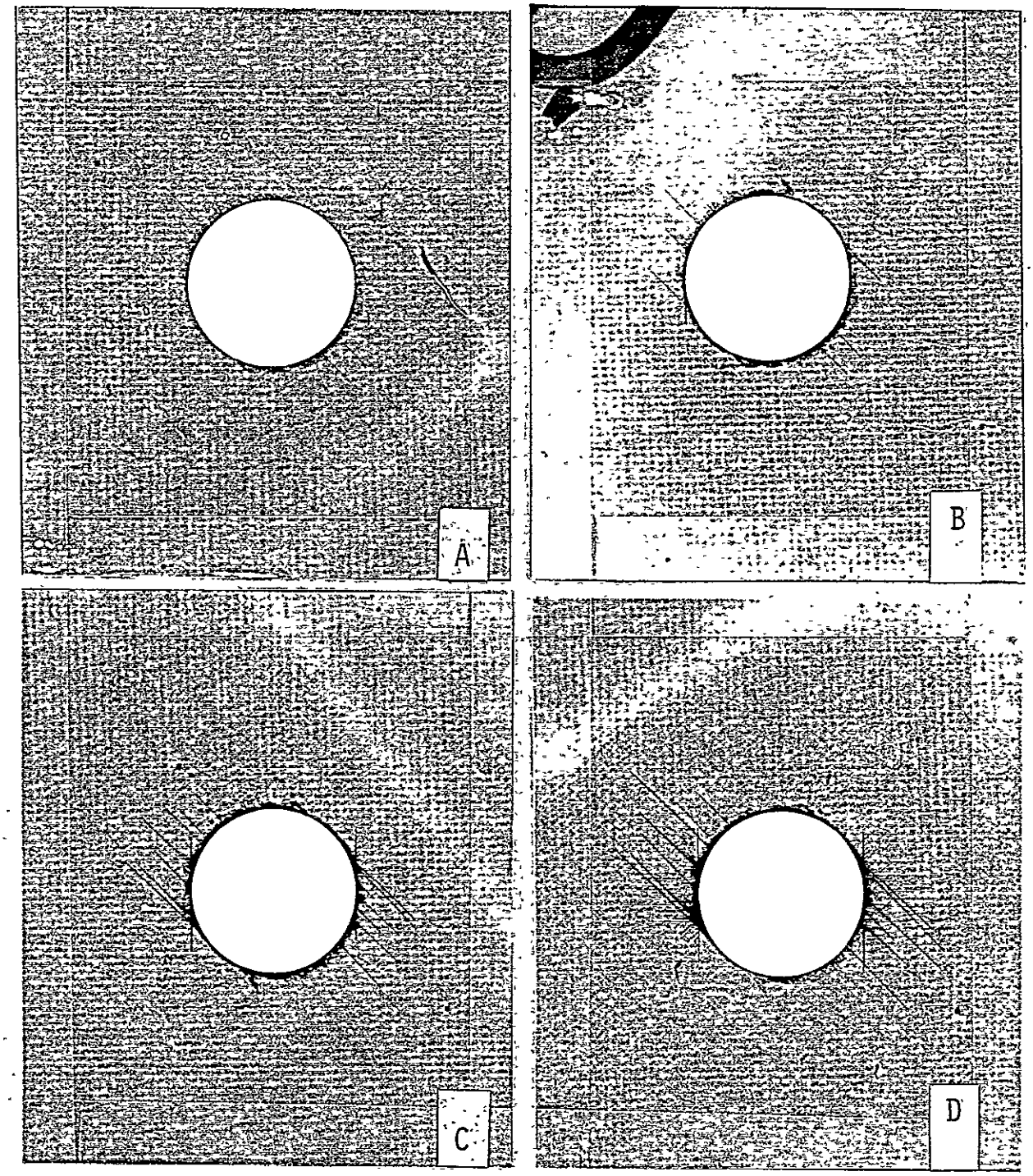

Figure 9: Quasi-Static Damage in a B-Laminate

appear, while the tangent zero-deg cracks are accompanied by similar cracks in the -45-deg direction. The spacing of the cracks in the -45-deg plies is less than that of cracks in the 90-deg plies. Observing the radiographs recorded at the 60 percent load level through a stereo-microscope reveals very small delaminations in regions where matrix cracks have formed. These delaminations are more apparent in subsequent radiographs made at greater loads.

The 80 percent load level radiograph, Fig. 9c, shows some additional +45-deg cracks located in the area between the very first cracks and those which followed, and the zero-deg cracks are longer. The delaminations are on the 45/90 interface in the region $\theta \simeq 100$-deg and $\theta' \simeq -80$-deg. Delaminations also occur on the 90/-45 interface.

Loading to 90 and 95 percent causes continued growth of the tangent zero-deg cracks away from the delaminated region and increases the intensity and size of the shadowed area. The number and extent of cracks in the 90- and -45-deg plies also increases. At the same time only one of the straight edges develops +45-deg cracks, Figure 9d.

Until the 110 percent load level is reached, all primary +45-deg cracks increase in number and length with respect to their associated secondary 90-deg cracks. At a load level

of 115 percent of the mean tensile strength, the first pair of cracks, one developing from the hole, the other from the straight edge, grow together and form a single, continuous crack, Figure 10a.

Cracks in the 90-deg plies initiate along the edge of the specimen at locations such that, in a plan view, they shape triangles defined by themselves, the free edge and the already present +45-deg cracks in the adjacent ply.

In the radiographs for the 125 percent and the 130 percent loads, Figure 10b, edge initiated damage, consisting of 90- and +45-deg ply cracks, can be seen.

The specimen broke while applying a 135 percent load level. Until then, the damage pattern consisted of matrix cracks with a major extent only in the zero-deg and the +45-deg plies and in the 90-deg plies only where +45-deg cracks did not develop. The delaminations extended as far as the two tangent zero-deg matrix cracks.

We may suspect an interaction between these zero-deg cracks, the delaminations, and the plus 45-deg matrix cracks which were seen on the 60 percent radiograph.

3.1.2.2 Fatigue Damage Patterns

First, consider fatigue damage due to the low load level of 70 percent, applied to specimen B-11. Comparing the radi-

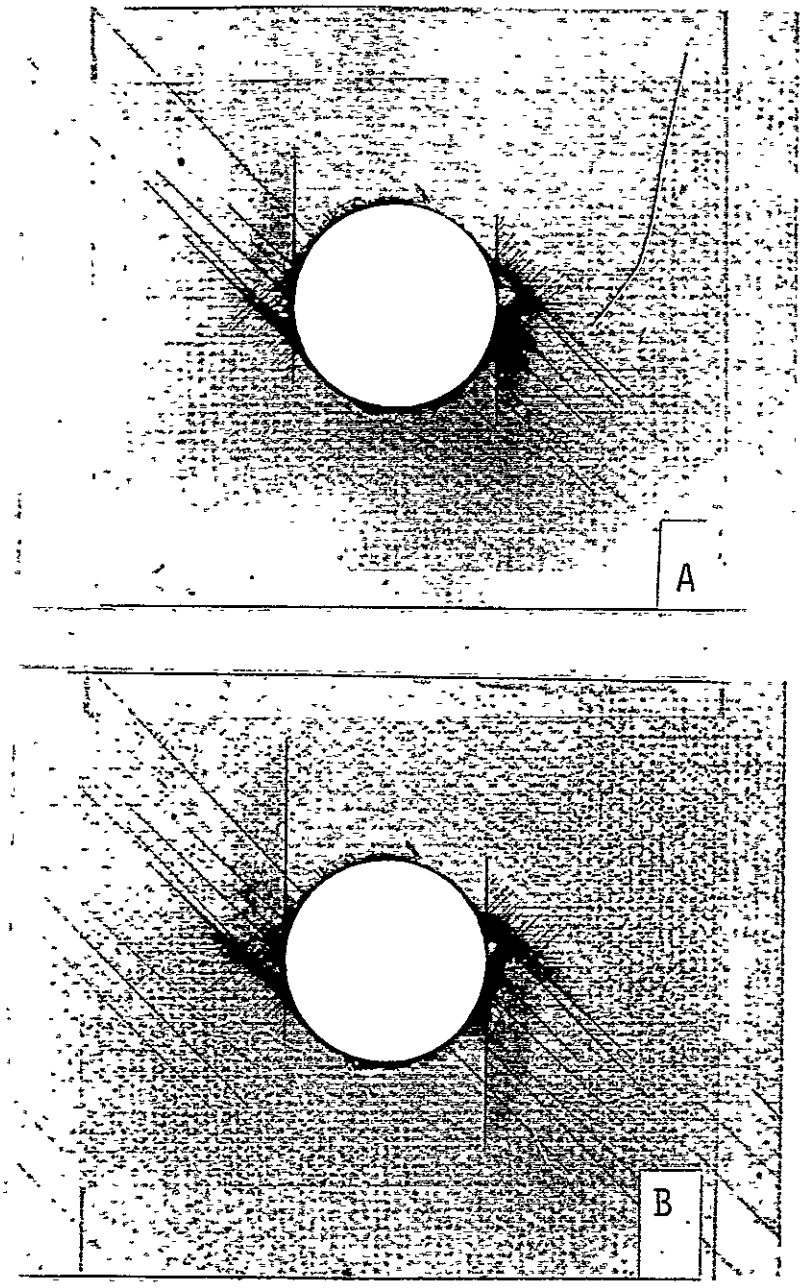

Figure 10: Quasi-Static Damage in a B-Laminate

ographs of B-11 with that of B-16 after applying the 50 percent load level (Fig. 10a) it is noted that the only visible damage in B-16 does not occur in the B-11 during its whole life.

The damage states of B-16 after the 70 percent load level and B-11 after 100 cycles (Figure 11a) at that load level are similar. Although the major or primary cracks in the zero-deg and plus 45-deg directions are comparable in number and length, the fatigued specimen developed more and longer secondary cracks than the quasistatically loaded specimen, and the delaminations are more distinct. After one thousand cycles, all previous damage modes are increased, but there are no new damage modes (Figure 11b).

The radiograph taken after ten thousand cycles shows the two symmetric, zero-deg cracks now having the length of the hole diameter. The tips of the primary plus 45-deg cracks extend as far along the longitudinal direction of the specimen as the zero-deg cracks. The secondary cracks in the minus 45-deg and 90-deg directions now form a dense mesh. The four original delamination areas grew together, extending from the hole edge along the zero-deg cracks and the darkest and longest 45-deg cracks. One of the two edges has a damage pattern consisting of 45-deg/90-deg crack combinations, each forming a little triangle, Figure 11c.

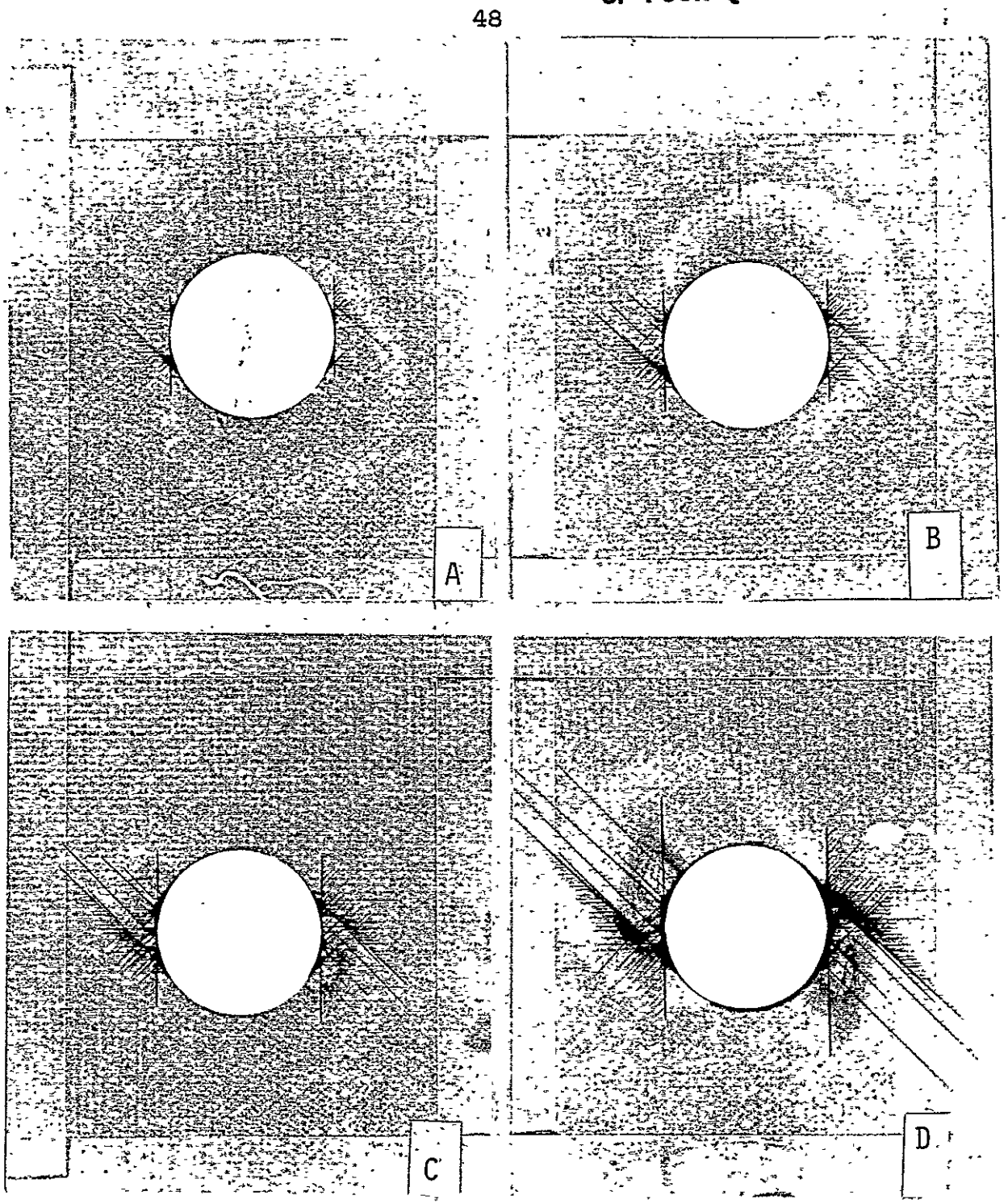

Figure 11: Fatigue Damage at Low Load Level in a B-Laminate

After one hundred thousand cycles the primary plus 45-deg cracks doubled in length while the tangent zero-deg cracks extend into the direction of advancement of the cracks in the 45-deg plies. Delamination now fills the region between the hole edge and the zero-deg cracks and, between these cracks and the straight edges, follows them very precisely. Delamination extends in the direction of the plus 45-deg cracks which are nearly tangent to the hole edge. At the previously damaged straight edge, the plus 45-deg cracks became longer, as shown in Figure 11d.

The last recorded state of damage at one million cycles shows the primary plus 45-deg cracks connecting the hole and the straight edges. The zero-deg cracks have a length of twice the hole diameter and form a boundary for one set of delaminations. Another delamination follows—the path of the plus 45-deg cracks as described previously, now covering about two thirds of the distance to the straight edge, Figure 12.

The strength test performed on the damaged specimen gave a very high residual strength of 137 percent of the mean initial strength of B-specimen, thus indicating that this radiograph shows a very advanced state of matrix damage and delamination while most of the load carrying fibers are still intact.

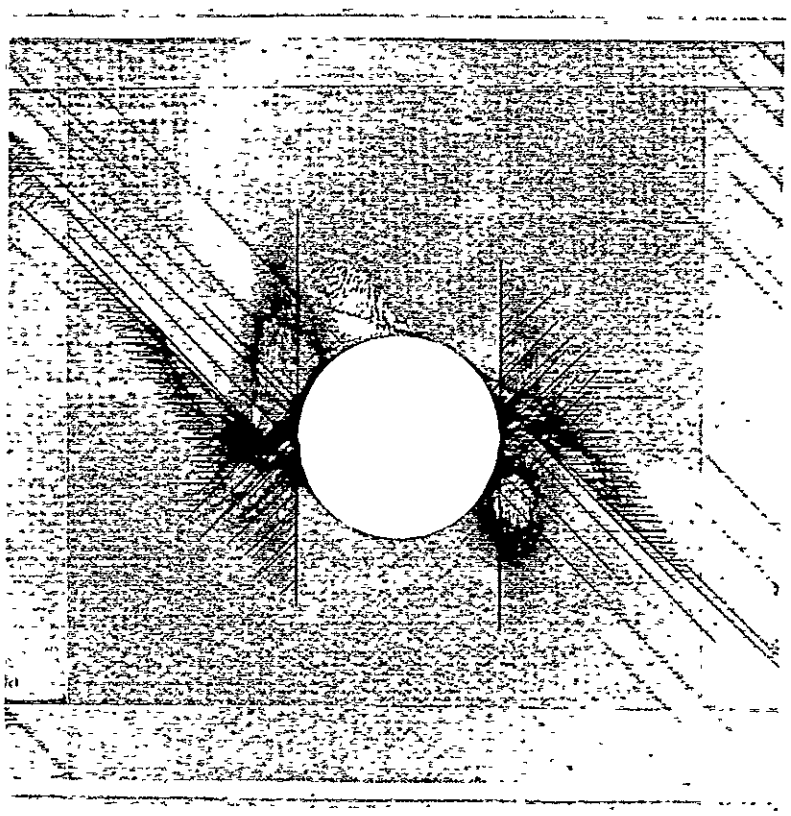

Figure 12: Fatigue Damage after 1 Million Cycles in B-11

3.1.3 Fatigue Damage at High Load Level

The state of damage in B-6 cycled ten times at 95 percent of the initial strength value is shown in Figure 13a. The damage state is very similar to that of B-16 after reaching the 95 percent load step. The only notable difference is the greater extent of the secondary 90-deg matrix cracks into areas of the cyclically loaded specimen which appear free of other cracks. Some of those cracks nearly reach the straight edge.

After one hundred cycles all cracks grew only a little while the delaminations spread out following the pattern indicated previously, as shown in Figure 13b.

The following nine hundred cycles produced an increase in the length of plus 45-deg cracks and an increase in number and length of the secondary 90-deg cracks, which reach the straight edges. Little damage initiates on these edges, as can be seen in Figure 13c.

Comparing the damage in the late stage of life of B-6 and B-11 (see Figure 11 and Figure 13d), the similarities consist of a nearly identical delamination pattern and the arrangement of the primary plus 45-deg and zero-deg matrix cracks. Although B-11 shows many straight edge induced matrix cracks in plus 45-deg, 90-deg, and minus 45-deg plies, B-6 has only a few of these cracks - an effect that

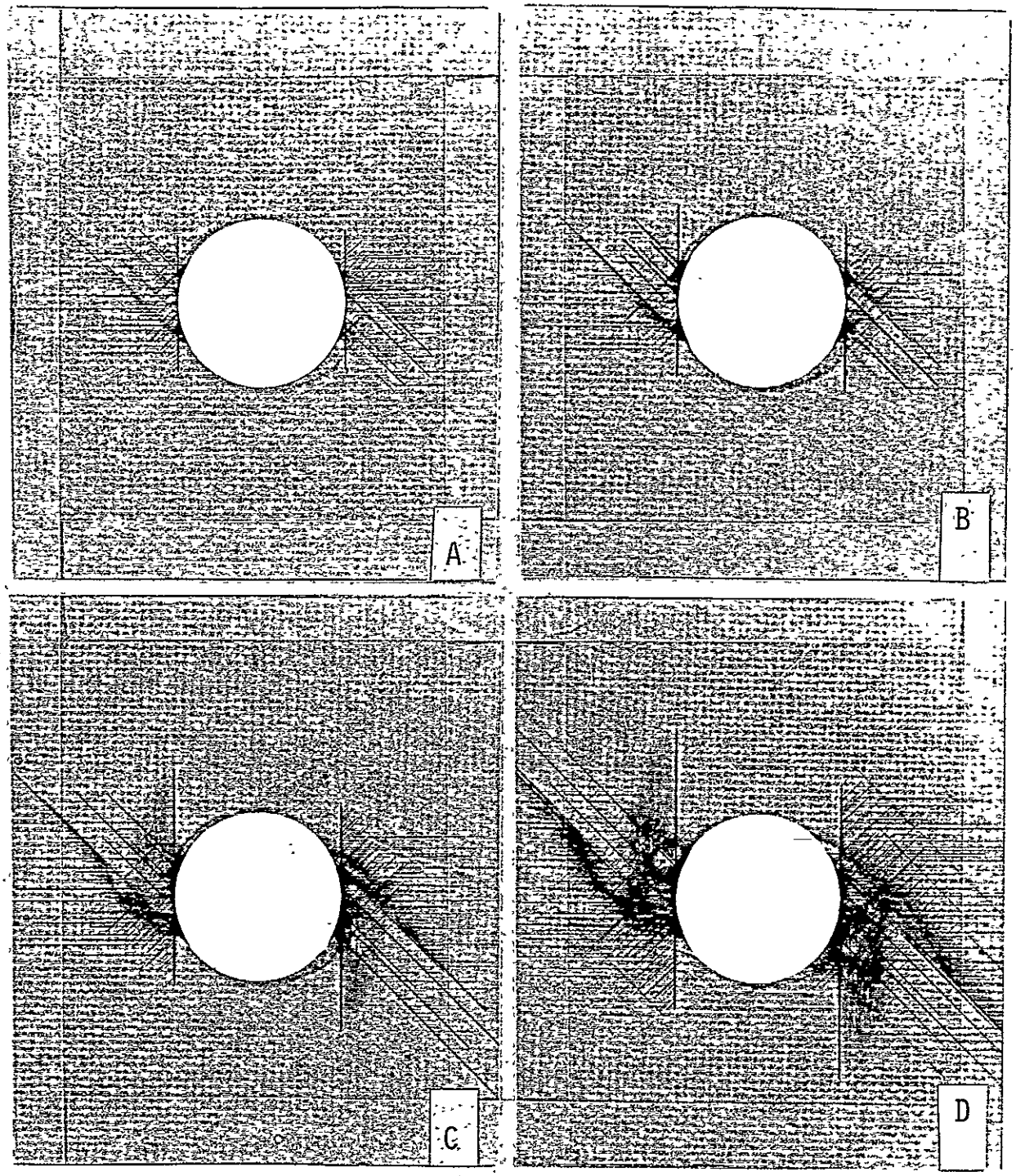

Figure 13: Fatigue Damage at High Load Level in a B-Laminate

is hard to explain due to the load levels. A possible cause of the difference might be a less careful finish (polish) of the B-11 edges, thus introducing additional local stress concentrations.

An additional effect in B-6 is the well developed pattern of secondary 90-deg cracks, most of which are near the straight edges. Another effect is the presence of large plus 45-deg cracks that neither belong to the primary cracks nor are initiated by them. This damage is probably a 'third order effect' in the sense that the new plus 45-deg cracks are initiated by the secondary 90-deg or minus 45-deg cracks or by the combined effect of these. Recalling that the plus 45-deg ply and the minus 45-deg ply are separated by the 90-deg ply, it is noted that interactive effects between cracks in separated plies may exist.

3.2 DEPLY TECHNIQUE

The deplied specimens A35 and B35 contain a maximum of damage. Both underwent continuous stiffness monitoring tests that were halted late in the fatigue life just prior to failure, see Figure 27. Figure 14 depicts the essential delamination pattern highlighted by stained areas on the interfaces of adjacent plies whose fiber orientation is indicated by the crossed lines. Since the stain comes from

zinc iodide concentrations, the outer limits of these areas mark the extent of delaminations as well as the position of matrix cracks containing a relatively large amount of zinc iodide. Experience shows that it is difficult to deply two adjacent layers of the same fiber direction. It seems likely that there is no significant delamination between the layers adjacent to the laminate midplane since, because of the symmetry of both the loading and the geometry, interlaminar shear stresses are zero in this plane.

3.2.1 A-Specimen

The characteristic 'spider'-shape defined by the stained areas on the zero-deg/90-deg interface of the A-specimen marks the extent of delaminations. The central stripes between the tangent cracks are not locations of delamination growth since delamination has fully taken place already (see X-rays, Figure 7 and Figure 8). They are probably caused by the zinc iodide in the middle zero-deg cracks. The tangent zero-deg cracks did not leave such a trace. This seemingly inconsistent observation may be rationalized using the previously mentioned model based on the adhesive relations between the fluid and the solid material. The width of the tangent zero-deg cracks is larger than that of the middle cracks so that the fluid is not kept in the wider cracks.

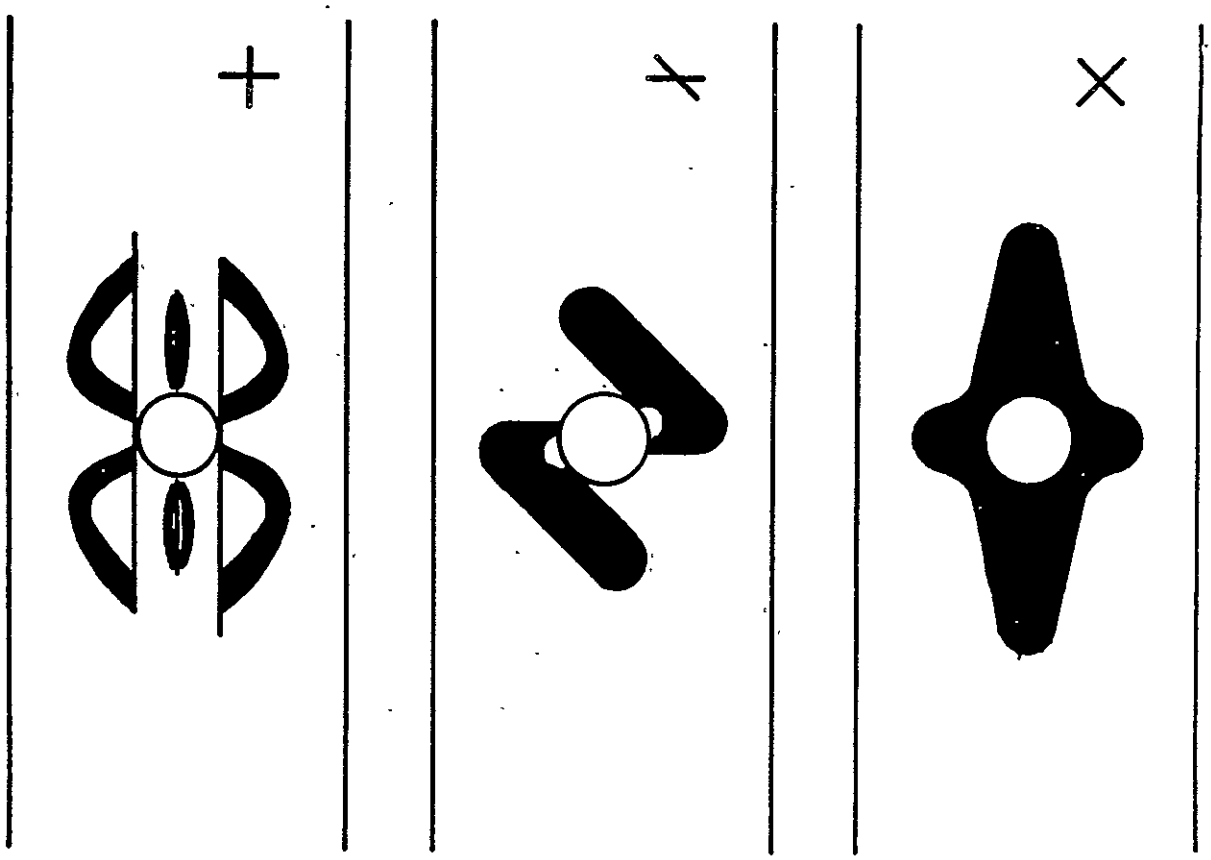

Figure 14: Delaminations on A-Laminate Interfaces

The interface between the 90-deg and the 45-deg layer shows a shadowed area resembling a 'Z'. This pattern can also be found on the X-ray in Figure 8. The typical pattern between the 45-deg and -45-deg plies is sketched in Figure 14.

3.2.2 B-Specimen

In contrast to the A-specimen, B35 was not treated with zinc iodide but was more thoroughly penetrated with gold chloride. However, delaminations can be identified and are sketched in Figure 15. Straight edge delaminations developed on the 90-deg/-45-deg interface. The larger extent of delaminations on the 45-deg/90-deg interface, compared with those on the 90-deg/-45-deg interface, indicates interactive effects between delaminations and matrix cracks. The shapes of delaminations on 45-deg/90-deg interfaces in the A- and the B-specimen, respectively, are quite different. While the larger extent of the cracks towards the straight edges in the B-specimen can be explained by the influence of matrix cracks in the outer layer, the larger extent of the delaminations in the A-specimen along the loading axis of the laminate could be related to buckling effects in this specimen. These buckling effects were visually observed during fatigue loading and are discussed in Section 4.4.2 on continuous stiffness monitoring tests. At the late stage of

lifetime of these deplied specimens, the delaminations cannot be related to the initial distribution of interlaminar stresses in the laminates.

3.3 MOIRE INTERFEROMETRY

All moire-fringe patterns show damage to the surface layer in detail and show the effect of damage on the surface displacement field. Although damage in the inner layers cannot be measured directly, its collective effect on the overall laminate response is included on the surface displacement. In other words, the moire technique is much more sensitive to damage in the surface layer than to damage anywhere else. For this reason, the fringe patterns of the damaged A-specimen and the B-specimen, respectively, look quite different. None of the photographs shows a perfectly undamaged laminate -- not even those taken under a 550 lb. load. Due to an error in the experimental procedure, the calibrated loading fixture was tested by loading specimens up to more than 1000 lbs. As a check on the accuracy and sensitivity of the experiments, the mean stiffness value from a series of static stiffness tests performed using a 1.0 inch extensometer was compared with an equivalent stiffness calculated from the fringe pattern. Two points, 1.0 inch apart, located symmetrically with respect to the transverse

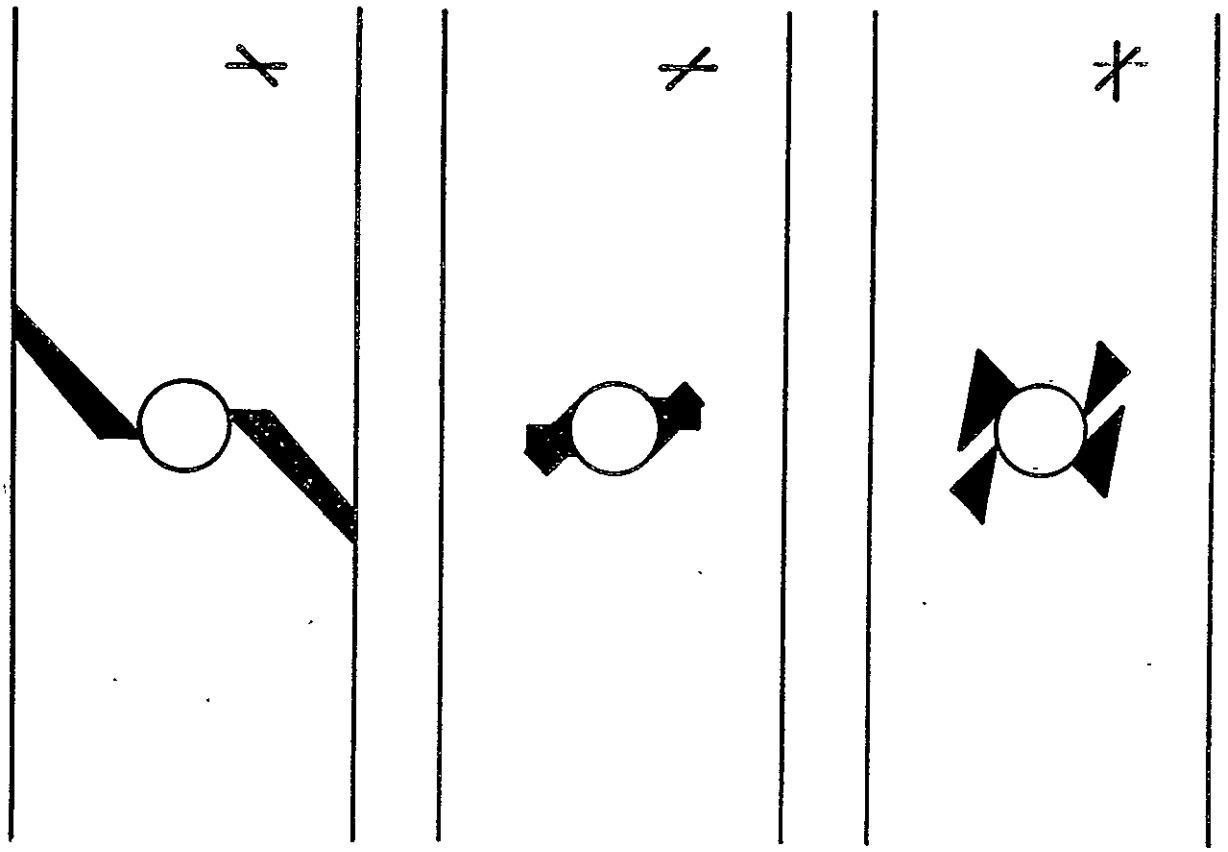

Figure 15: Delaminations on B-Laminate Interfaces

axis of the specimen were taken and the number of included fringes was counted. This number was corrected by a low-load fringe order and gave a stiffness of 53.3 msi and 51.8 msi for the A- and B-specimens, respectively. Both values lie within the range of the 1.0 inch extensometer measurements but are about 6 percent and 4 percent greater than the mean value of these measurements, respectively. There is an agreement between the results of the two methods in that the initial stiffness of an A-specimen is slightly higher than that of a B-specimen. Since the part of the specimen reproduced on the moire negative is small, it was not possible to compare the 2.0 inch and the 3.625 inch extensometer measurements with values obtained from the fringe pattern. At a distance from the hole edge of less than two diameters, the longitudinal displacement field appears to be almost uniform. Another demonstration shows that the 1.0 inch extensometer stiffness measurement is almost insensitive to eccentricities of the extensometer with respect to the hole. For the A-specimen, for instance, a shift of 0.1 inches led to a fringe order deviation of 2 from the correct value of 97.

3.3.1 A-Specimen

3.3.1.1 Fringe Pattern of the Undamaged Specimen

The fringes for the longitudinal (u) and for the transverse (v) displacements are shown in Figure 16a and b, respectively. One of the four matrix cracks tangent to the hole is not yet fully developed and in this area the highly increased density of the u-displacement fringes can be studied. On the opposite side of the hole, along the zero-deg matrix crack, the fringes are less dense than in the area spoken of above. At a distance from the hole edge of less than two diameters, the u-displacement field appears to be almost uniform.

3.3.1.2 Onset of Fatigue Damage

Figures 17a and b show the damage state of the specimen under 1050 lbs load before the load is cycled and that of the specimen after 10 cycles at 1550 lbs maximum load, respectively. After 10 cycles of fatigue loading, the crack that was not fully formed in the specimen before cyclic loading has grown, and its immediate effect on the stress field close to the hole edge can be studied. Apparently the crack redistributes and relaxes the strain field and lowers the strain concentration. From the results of an elastic analysis of an isotropic plate with a circular hole under

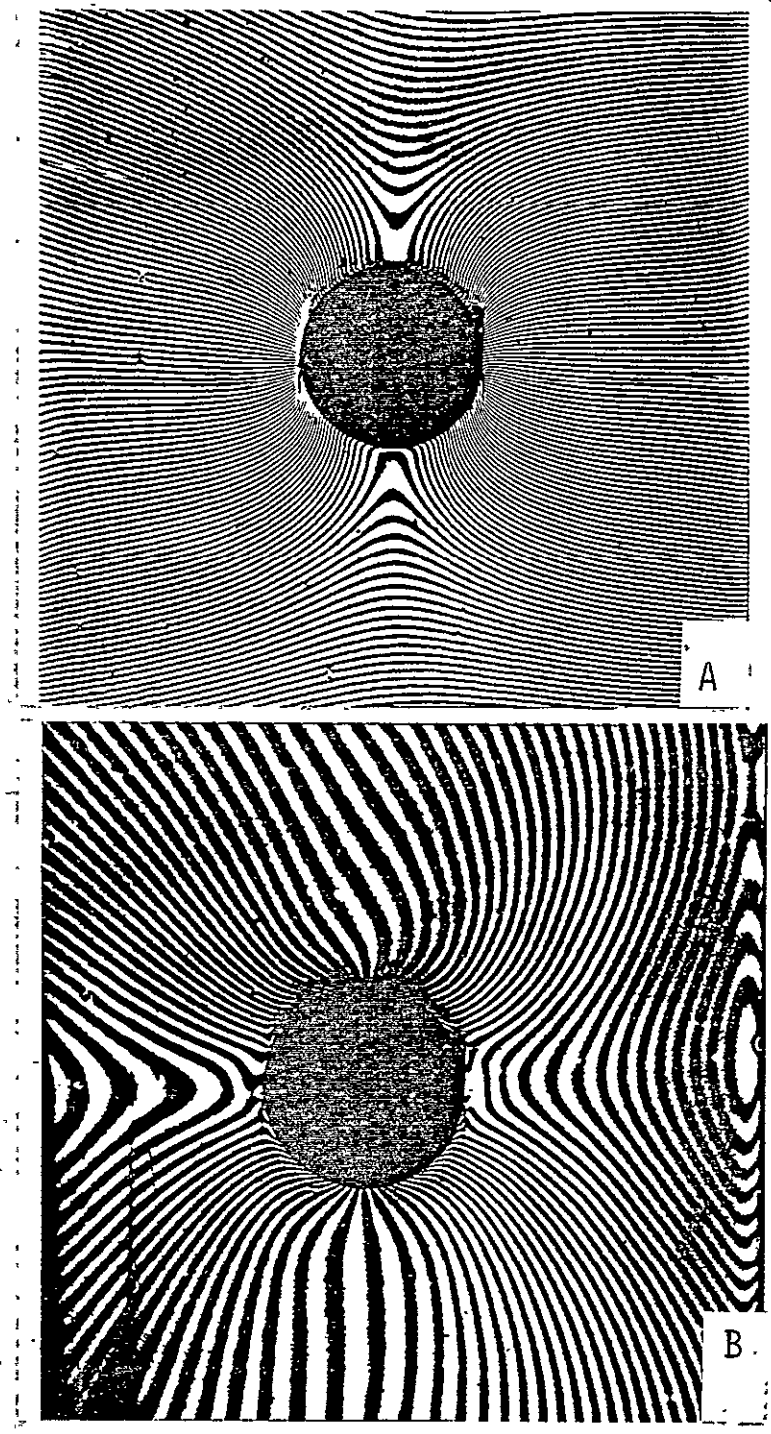

Figure 16: Fringe Patterns of an Undamaged A-Laminate

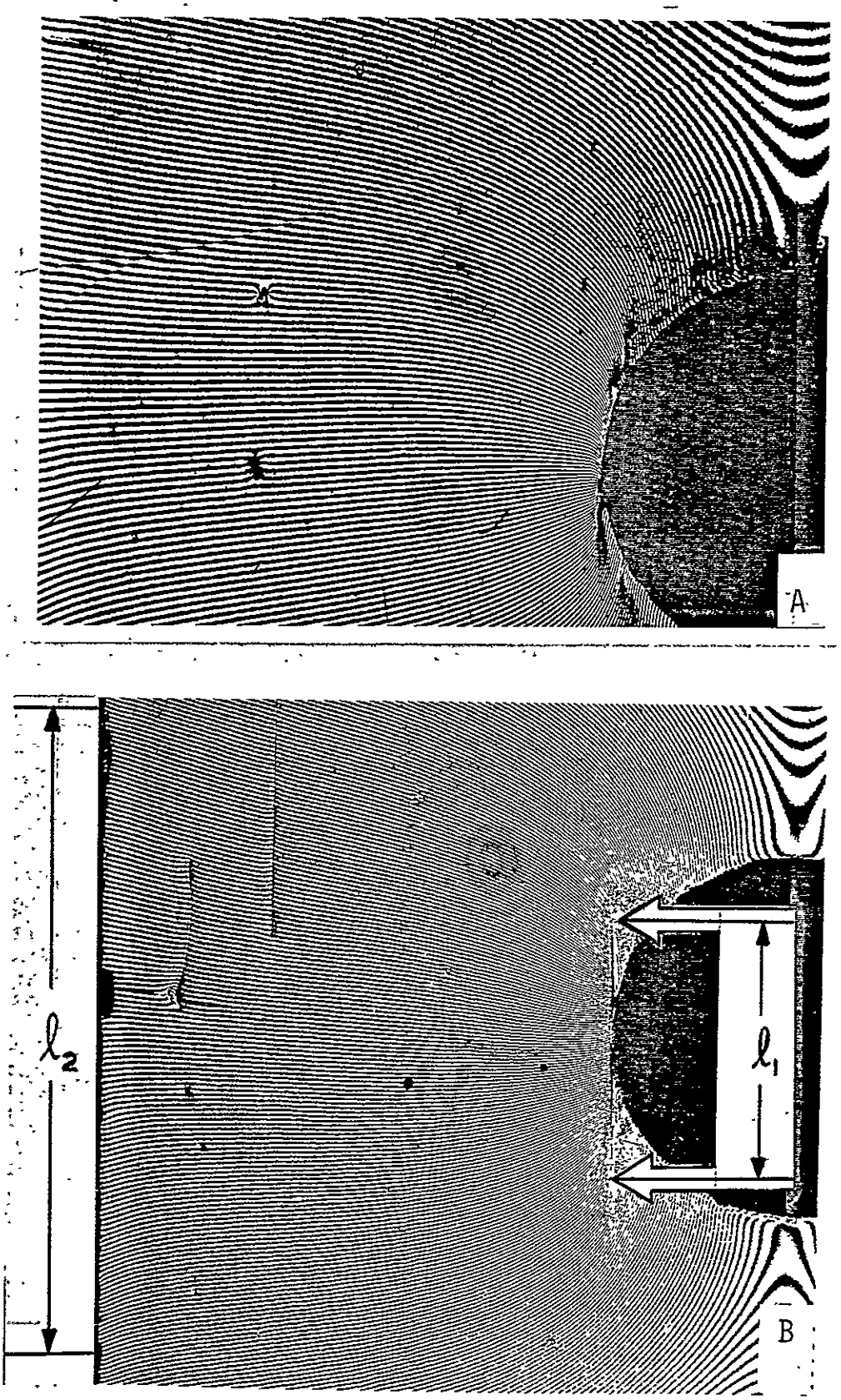

Figure 17: Fringe Patterns for an Undamaged and Slightly Damaged A-Laminate

uniaxial tension, a strain concentration of three for ε_x may be assumed for an idealized, undamaged situation and compared with the new strain concentration along the crack. It is difficult to determine the maximum fringe density at the crack. Therefore, fringes emerging from the crack tips are traced to a straight edge where the distance between them is measured. This value, in comparison to the crack length, serves as an averaged strain concentration, although the actual value of strain concentration at the crack tip may be greater. The relation between the relaxation of strain at the tangent cracks and the strain distribution along the straight edge can be determined by relating the length a chosen segment to the number of fringes within this segment. This procedure should lead to correct numbers even under the condition of frequency mismatch by subtracting the null-field fringes.

3.3.1.3 Fringe Pattern of the Highly Damaged Specimen

Figures 18a and b clearly show the areas of delaminations between the zero-deg matrix cracks and the influence of the damage on the lamina behavior. The former complete symmetry of the fringe pattern is now reduced to a mere point symmetry with respect to the specimen center. Looking at the photograph, the crack above the hole is shifted toward the

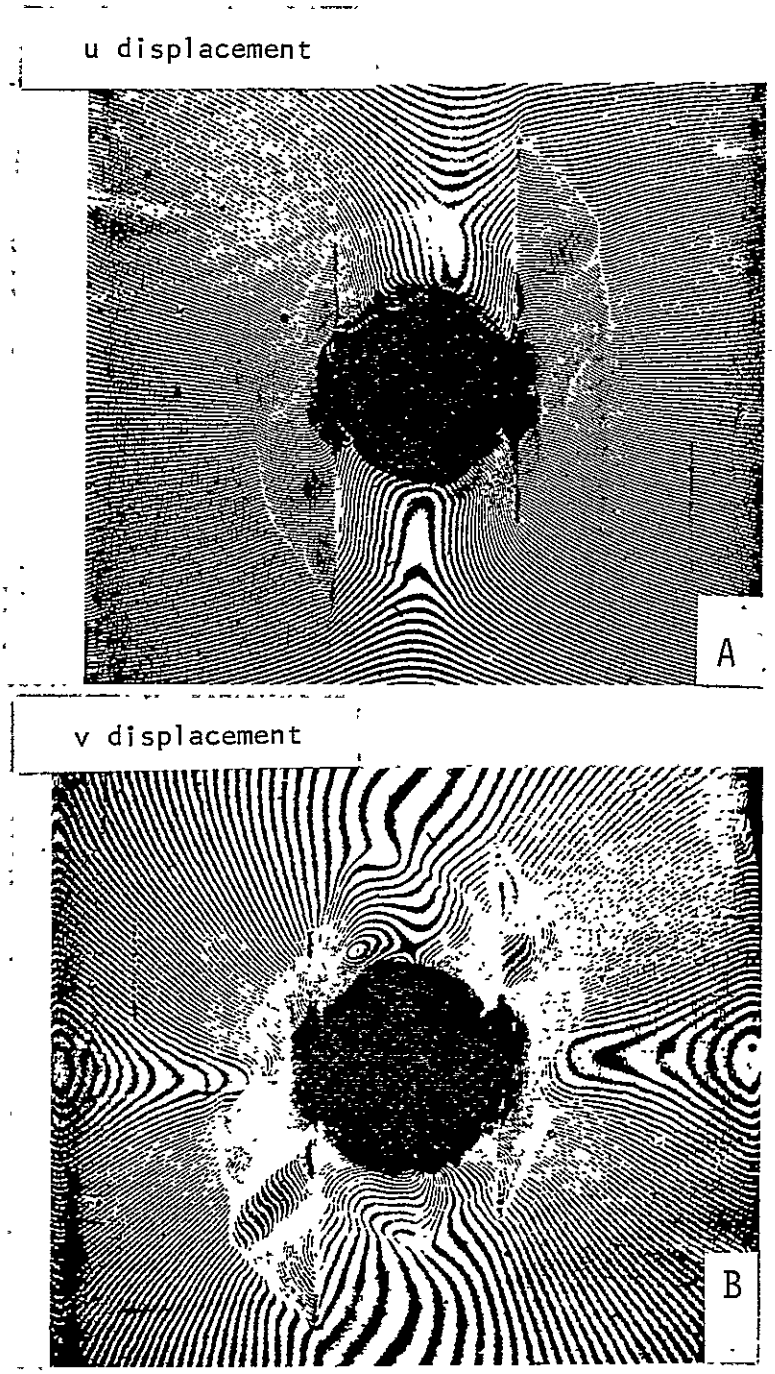

Figure 18: Fringe Pattern of the Highly Damaged A-Laminate

negative x-direction (loading direction) while the areas of low strain are shifted clockwise, possibly an effect of damage in the 45-deg plies. The tongue shaped areas bounded by the hole edges and the tangent cracks undergo a relative displacement to the delaminated areas outside the cracks. Although the edge of the hole appears somewhat diffuse, it can be seen that the strain concentration factor for ε_x is approximately uniformly distributed over the whole length of the cracks with only slight additional concentrations at the tips of the cracks. As an estimate, the average strain concentration along the cracks is 1.46 and that at the tips is not determinable. Considering a fringe-order difference of 149 between the idealized 1.0 inch extensometer measurement points minus 24 fringes of residual deformation found on the null-field pattern and an applied load of 550 lbs., a stiffness value of 79.5 percent of the value calculated for the undamaged specimen is determined.

3.3.2 B-Specimen

3.3.2.1 Fringe Pattern of the Undamaged Specimen

The initial fringe pattern of the B-specimen is almost undisturbed by cracks as Figures 19a and b show. It seems that at this stage only the tangential +45-deg cracks (here depicted in -45-deg direction) lead to a significant reduction of the strain component ε_x at the hole edge.

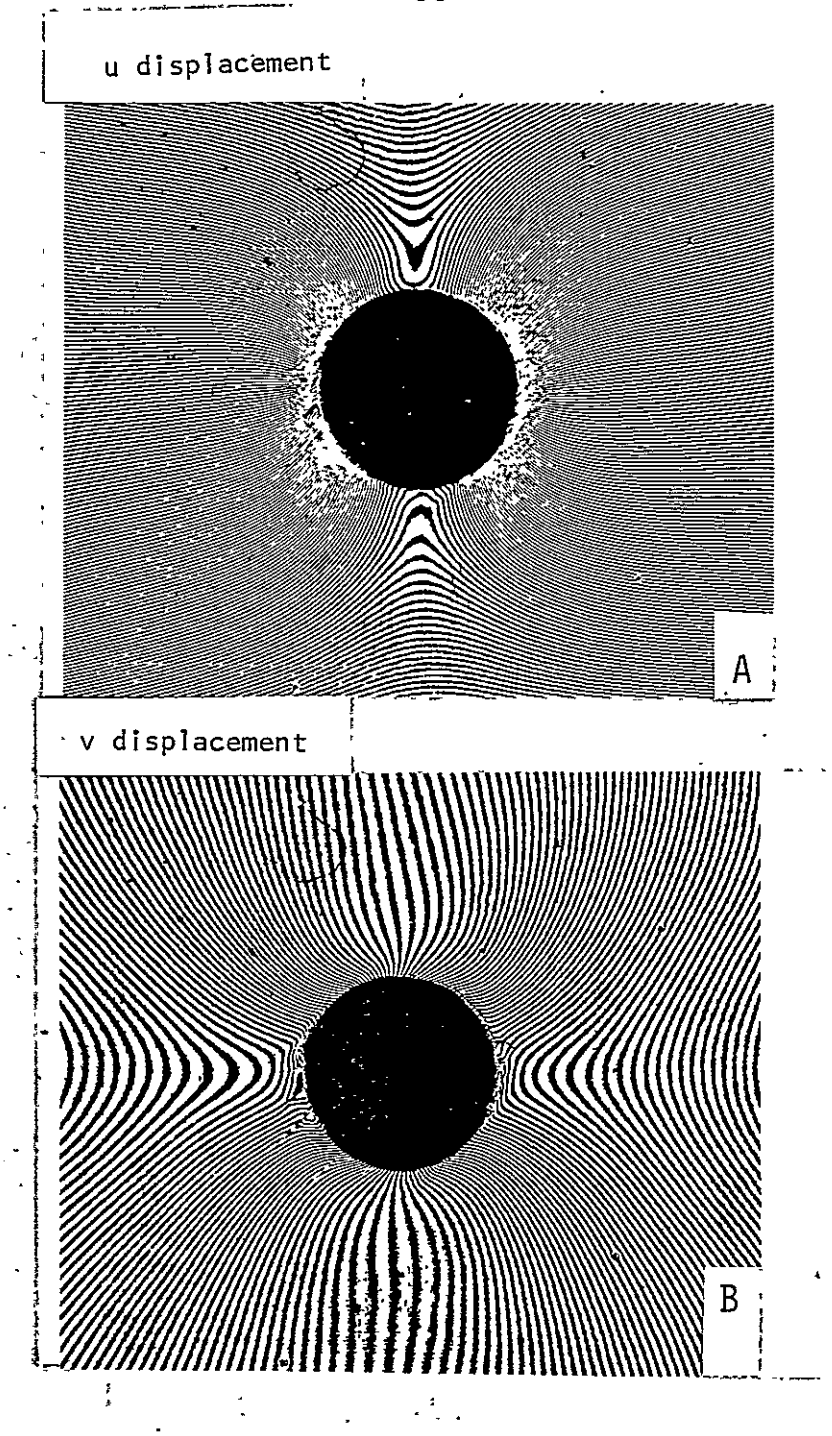

Figure 19: Fringe Pattern of an Undamaged B-Laminate

3.3.2.2 Onset of Damage

Figures 20a and b indicate that the displacement field is heavily changed at locations where cracks are almost perpendicular to fringes and only slightly changed where cracks are almost parallel to the fringes. The displacement field is most changed by the cracks tangent to the hole. A greater change in the displacement field corresponds to a greater stress relaxation and, going one step further, to a greater reduction of the elastic energy due to the regional stiffness of the laminate. In this context, the X-ray photos document a more rapid growth of the tangent +45-deg cracks than of the other +45-deg cracks after the onset of damage.

3.3.2.3 Fringe Pattern of the Highly Damaged Specimen

Figures 21a and b show the delaminated areas along the tangent +45-deg cracks. It is difficult to obtain a 1.0 inch extensometer equivalent stiffness since the large +45-deg cracks make it impossible to count fringes through this area. Particularly in Figure 21b, the fringes have curvatures regularly placed along the +45-deg direction. A possible interpretation is that along these lines cracks are impending but not yet fully formed. Such regularly distributed fringe shifts appear also between the hole and the

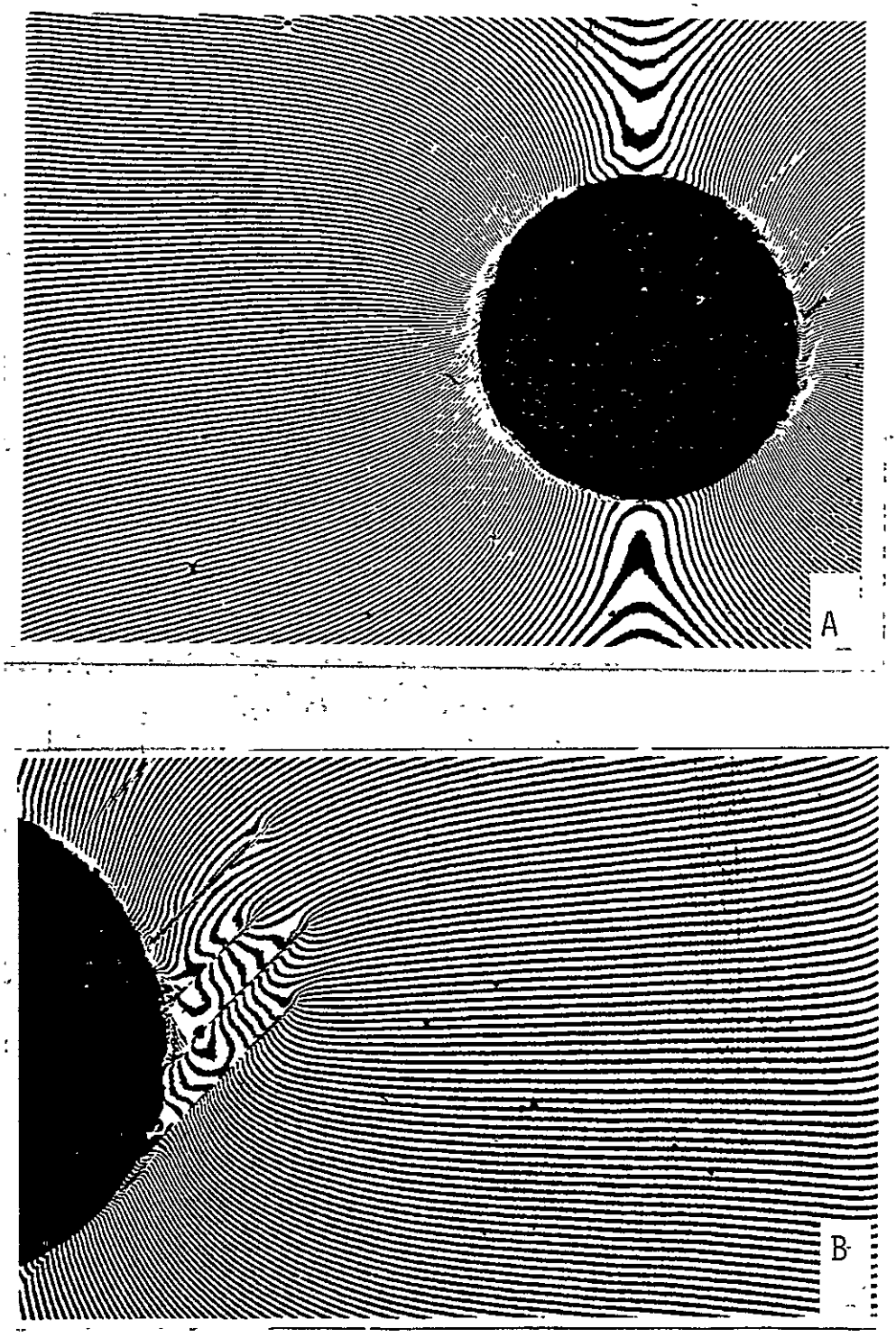

Figure 20: Fringe Patterns for an Undamaged and Slightly Damaged B-Laminate

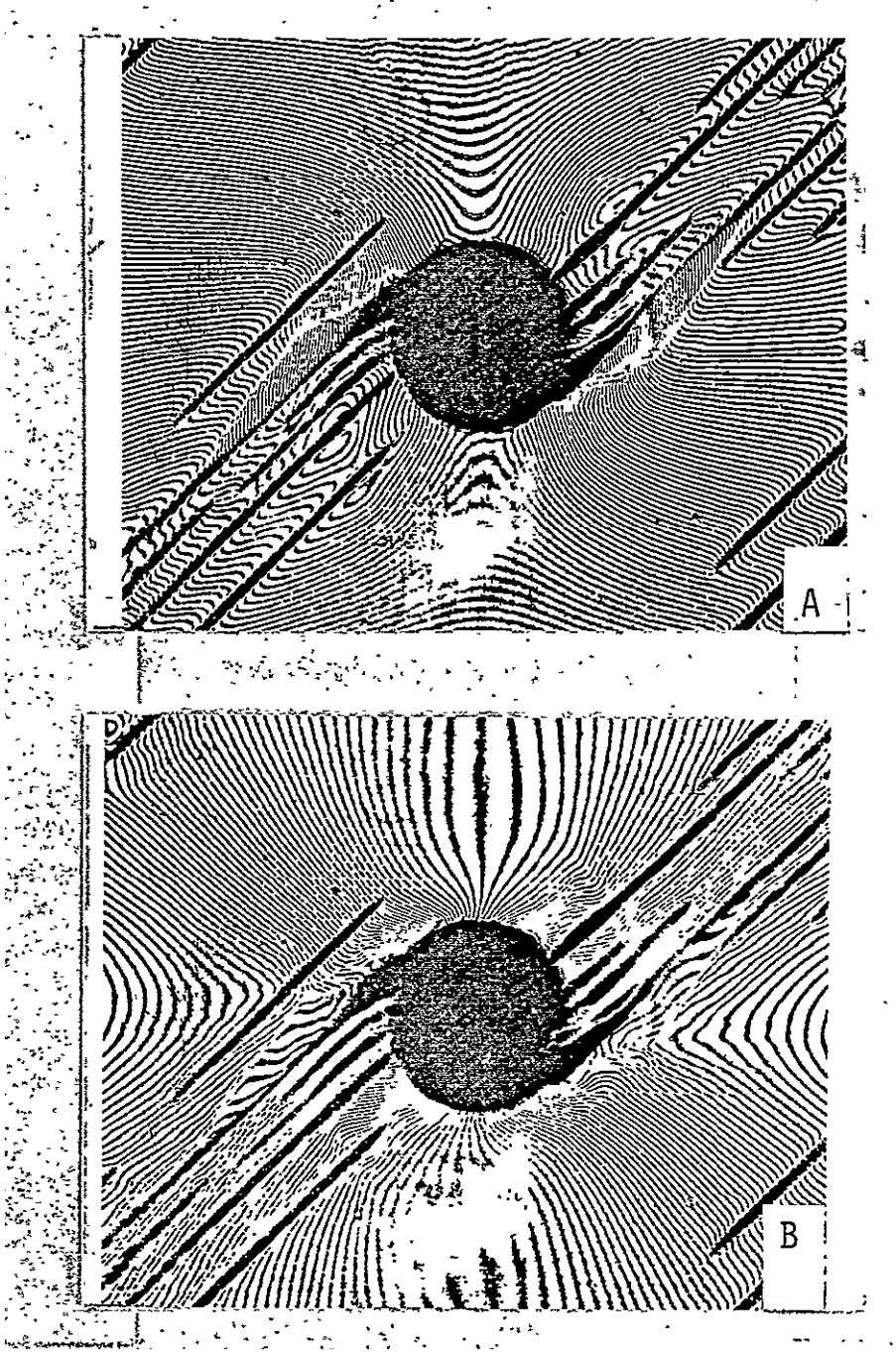

Figure 21: Fringe Pattern of the Highly Damaged B-Laminate

straight edge in the 90-deg direction. It is possible that this fringe pattern shows a local displacement which precedes crack initiation or, in the case of a fringe shift along a 90-deg direction, the pattern is due to a crack in the adjacent layer. Unlike the fringe pattern of the A-specimen, fringe patterns of the B-specimens do not provide data to make quantified estimates on the residual strain concentration, since the strength governing zero-deg layers is located at the midplane of this laminate.

IV

4.0 RESULTS

4.1 INITIAL TENSILE STRENGTH

Tensile strength tests were performed on five specimens of each type of laminate, including the unnotched laminate.

In Figure 22, the failure load of each specimen is represented by the length of a vertical line. The mean failure loads of A,B and C specimens were 2620, 2240, and 4680 lbs., respectively, as indicated by the solid horizontal lines.

The lower, dashed horizontal lines indicate the mean load levels for which major discontinuities in the load-strain curves, as well as the first strong acoustic emissions during the loading process, occurred. The percentages refer to the mean failure load of each type of laminate. The C-specimens typically had edge induced delaminations accompanied by strong acoustic emissions at approximately 0.66 percent strain. The correlation between the onset of acoustic emission activity and this strain value was much better than that with load values. The root of the sum of the squared deviations is 2.54 for the strains and 5.59 for the corresponding loads.

After the delamination point, indicated by an increase in strain for nearly constant load on the load-strain curve,

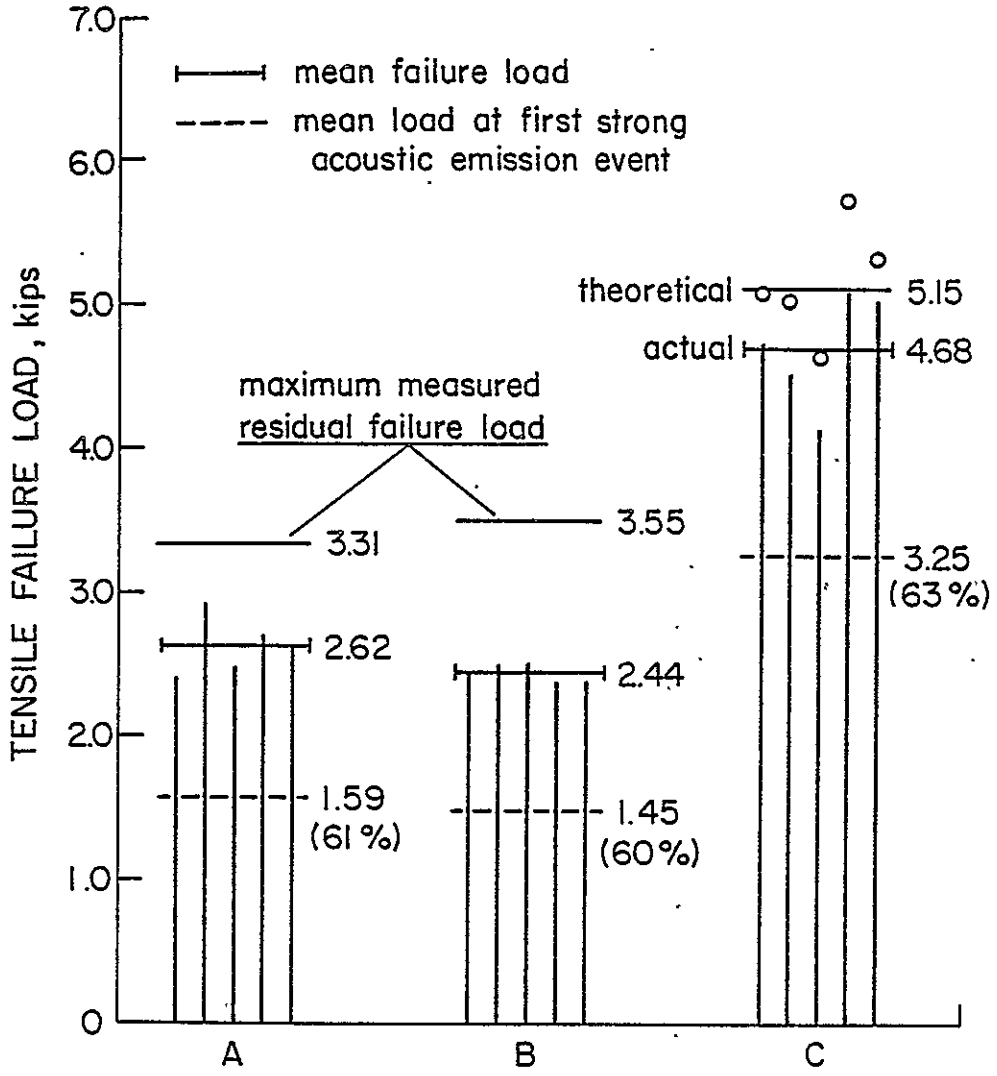

Figure 22: Static Tensile Strength

the stiffness was reduced. Both the step in the curve and the reduced slope after the step suggested the idea of predicting strength values for the 'no delamination' situation by simply multiplying the mean stiffness value taken from the initial part of the load-strain curve by the failure strain of each specimen. These values, indicated by the open circles, average to 5150 lbs. or 110 percent of the actual mean strength as indicated in the figure. Considering the critical, net cross sections, which are the notched sections for the A and B specimens, the average failure stresses are 52.8, 48.6 and 71.5 ksi for A-, B-, and C-specimens, respectively. The large difference between the strength values of notched and unnotched specimens is due to the stress concentrating effect of the hole. Yet, it must be noted, that the strength of the C-specimens is also reduced by straight, free edge effects. However, the strength values indicate that a strength reduction factor for the hole must be much larger than that for the straight edge.

Furthermore, since edge effects in general (whether for curved or straight edges) decrease rapidly with increasing distance from the edge, the effects of the straight and the curved edges on the notched laminates are independent. In other words, we may assume that for the notched specimens used in this study, the effects of the straight edge do not

yield an additional contribution to the reduction of static strength caused by the hole.

It is important to note that the greatest measured residual strengths, related to the notched cross section, of A- (66.5 ksi) and B- (71.4 ksi) specimens approach the tensile strengths of C-specimens, thus indicating that fatigue damage redistributes local stresses to the extent of reducing the stress concentration due to the hole.

4.2 INITIAL STIFFNESS

Stiffness data were taken from the linear part of the load-strain curves recorded during the tensile strength tests by means of a 1.0 in. extensometer centered with respect to the hole. Each vertical line in Figure 23 represents the stiffness of a specimen. Mean stiffness values, based on the area of the unnotched section, are indicated by the horizontal lines. The stiffness values of A- and B-specimens, based on the unnotched cross-sectional area, are lower than the stiffness values determined for unnotched C type specimens. This demonstrates the large, local deformation field associated with the local stresses due to the hole.

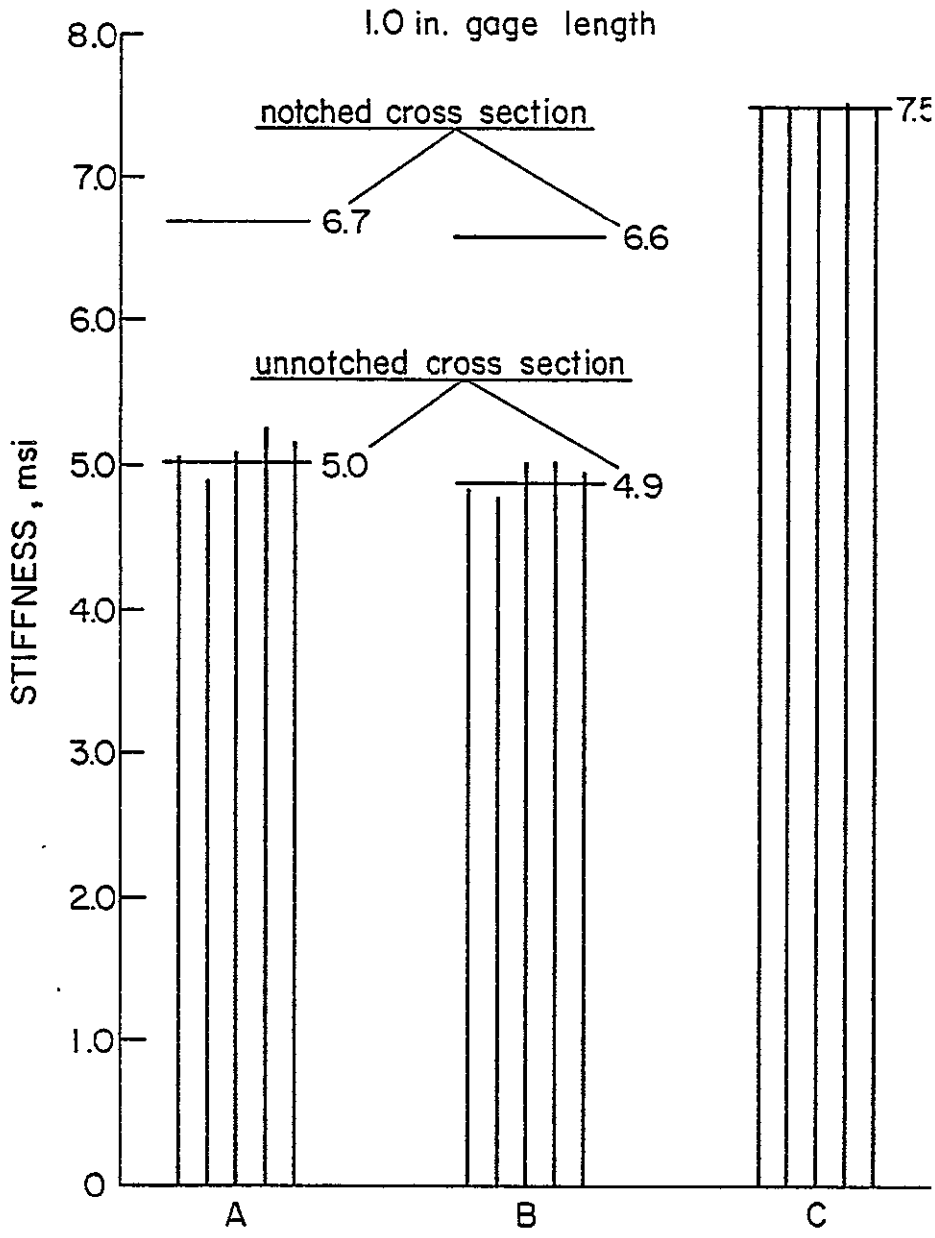

Figure 23: Static Stiffness

4.3 S-N DATA

A lifetime of more than 10^6 cycles under the condition of a sinusoidal load with a ratio $\sigma_{min}/\sigma_{max} = 0.1$ and a frequency of 10 Hz can be expected at an 80 percent load level (2095 kips) for A-specimens and a 70 percent load level (1710 kips) for B-specimens. Load-log life curves for the two laminates are shown in Figure 24. A-specimens, cycled at a 95 percent load level (2485 kips), and B-specimens, cycled on an 85 percent load level (2075 kips) will survive 10^5 cycles.

Two A-specimens had an average lifetime of 1.1×10^6 cycles at the 80 percent load level while the B-specimen, cycled at the 70 percent level, had a residual strength of 137 percent of the virgin strength after 10^6 cycles. The residual strength data for type B laminates suggest that residual strength values of this magnitude occur during the final decade of logarithmic life.

4.4 STIFFNESS DEGRADATION

4.4.1 Interrupted Stiffness Recording

Stiffness data for type B laminates cycled at the 85 percent level are shown in Figure 25. The two stiffness curves show the effect of gage length on the stiffness values. A clip type strain gage extensometer centered over the hole

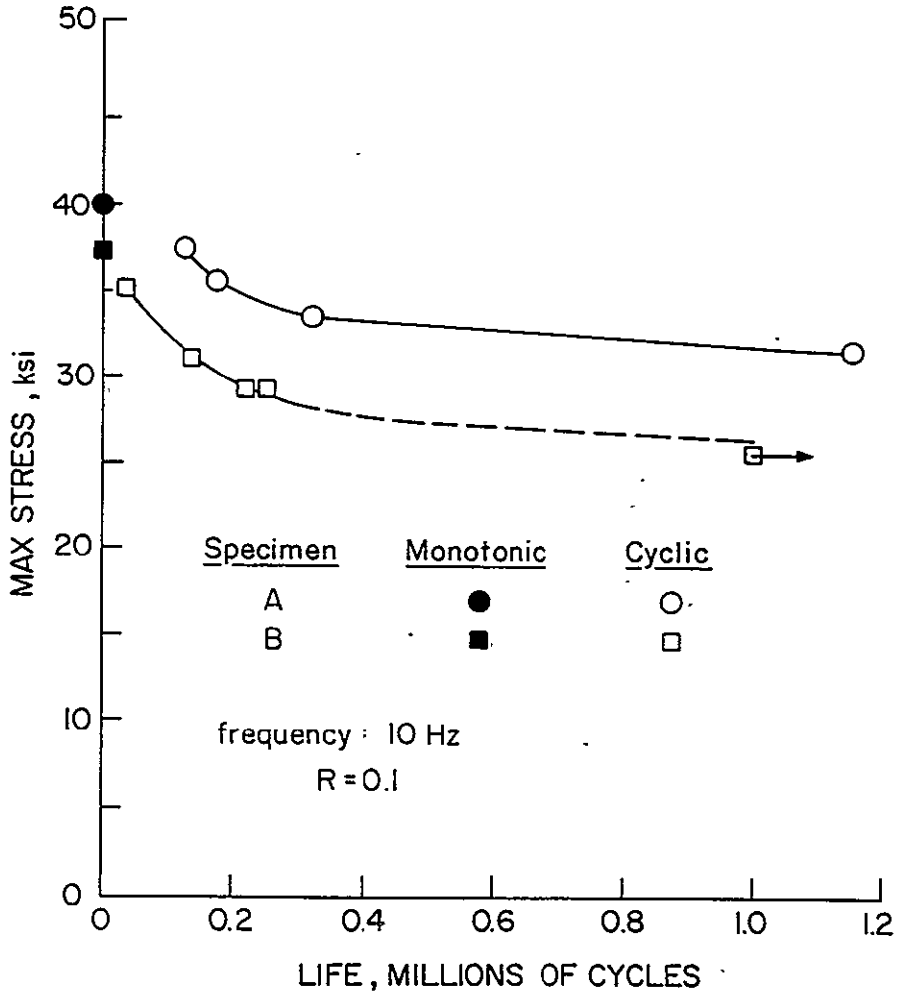

Figure 24: S-N Curves

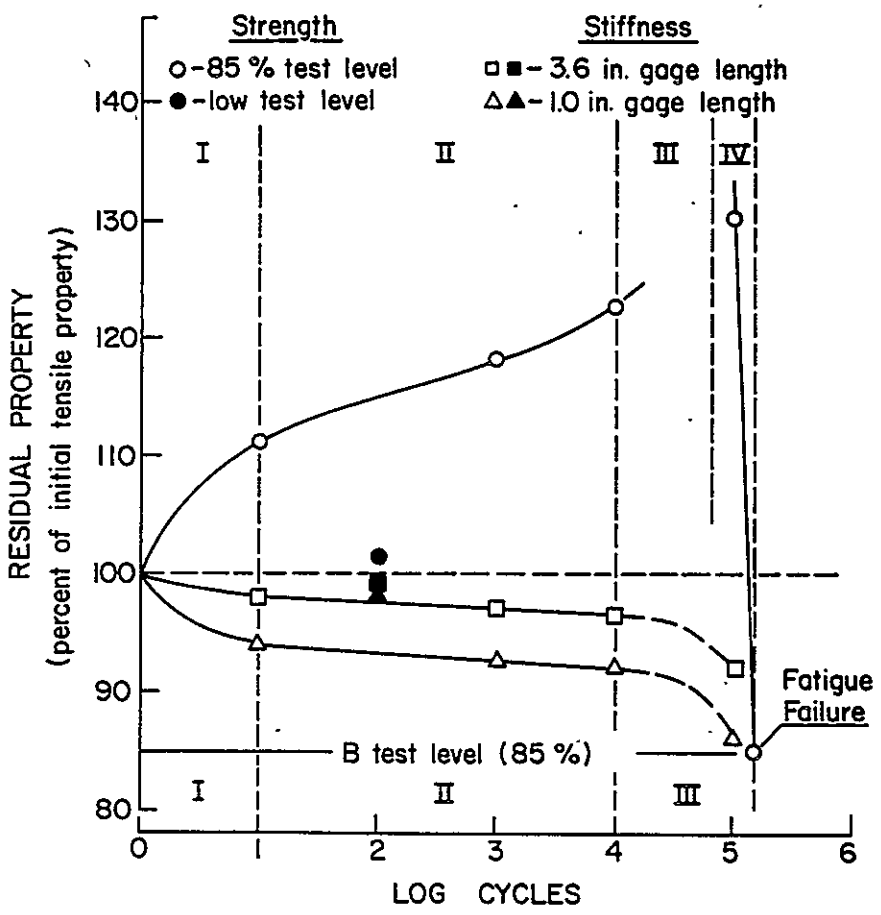

Figure 25: Stiffness and Residual Strength Versus Life

was used to measure displacement over a 1.0 inch gage length. A DCDT extensometer centered over the hole measured displacement over a 3.625 inch gage length. The stiffness change values based on the short extensometer data are larger. However, if the damage zone spreads outside the 1.0 inch gage length, the stiffness change values determined from the short extensometer are inaccurate.

The process of damage development around the hole of a type B laminate is indicated by the stiffness curves shown in Figure 25. The limits of regions I, II, and III are somewhat arbitrary, but are chosen to reflect transitions in the damage growth process as represented by stiffness change. In region I, the stiffness decreases at a decreasing rate as small matrix cracks develop near the hole. In region II, the stiffness degrades linearly with log cycles as the matrix cracks in the zero and 45 deg plies extend away from the hole and delaminations form in the region damaged by matrix cracks. Region III begins as the stiffness degradation rate increases. In this region, the sharp decrease in stiffness is associated with further extension of the cracks in the zero and 45 deg plies, an increase in the density of the cracks in the 45 deg. plies, and growth of delamination along the 45 deg. matrix cracks. Early in the life of the laminate (region I) the damage is confined to the approxi-

mate zone of stress concentration around the hole. In later stages of life, the stresses around the hole are redistributed and the stress concentration around the hole changes due to the growth of the damage zone away from the hole. Radiographs of damaged type B specimens at several intervals in the loading history are shown in Figure 11 and Figure 13. The data in Figure 25 are presented in terms of percent change in stiffness because the exact values of stiffness are not repeatable in situations where the cyclic test is stopped, the extensometer is removed from the specimen, and the specimen is removed from the grips for nondestructive evaluation at various cyclic intervals. However, if the stiffness values are determined at the beginning and end of each cyclic interval, or are recorded throughout a cyclic interval by the data aquisition system, the change in stiffness during the cyclic interval can be determined. The total change is then computed as the sum of the stiffness changes for all intervals.

4.4.2 Continuous Stiffness Recording

The plots of the results of the peak detector program on a logarithmic lifetime scale confirm the estimated stiffness curves based on quasi-static tests. The suggestion of a five percent stiffness loss after 100 cycles at a 90 percent

cyclic load for both laminates was taken into account by multiplying the first stiffness value received by the peak detector after 200 cycles, by the factor 0.95.

Figure 26 shows regions II and III of the stiffness degradation due to fatigue loading at the 90 percent load level. The time axis is logarithmically scaled. In this representation, region II appears as an almost linear line leading into a sharp knee which connects region II with region III. Immediately beyond the knee, the degradation rate appears to be highly increased. At the end of region III, the stiffness decay accelerates again until failure.

Comparing the two curves shown in Figure 26, the B-laminate shows less stiffness degradation before the knee, a later and more distinct knee, and a higher degradation rate after the knee than the A-laminate. The stiffness loss at the end of fatigue life is 18 percent for the B-specimen and 40 percent for the A-specimen. The data have been replotted using a linear scale for the life axis, Figure 27. Throughout the lifetime, the A-specimen has a lower stiffness than the B-specimen. Between 10 K and 50 K cycles, the degradation rates of both curves are similar; after that the A-specimen looses stiffness more rapidly than the B-specimen. Although the total stiffness loss during its lifetime is lower for the B-specimen, its degradation rate shortly

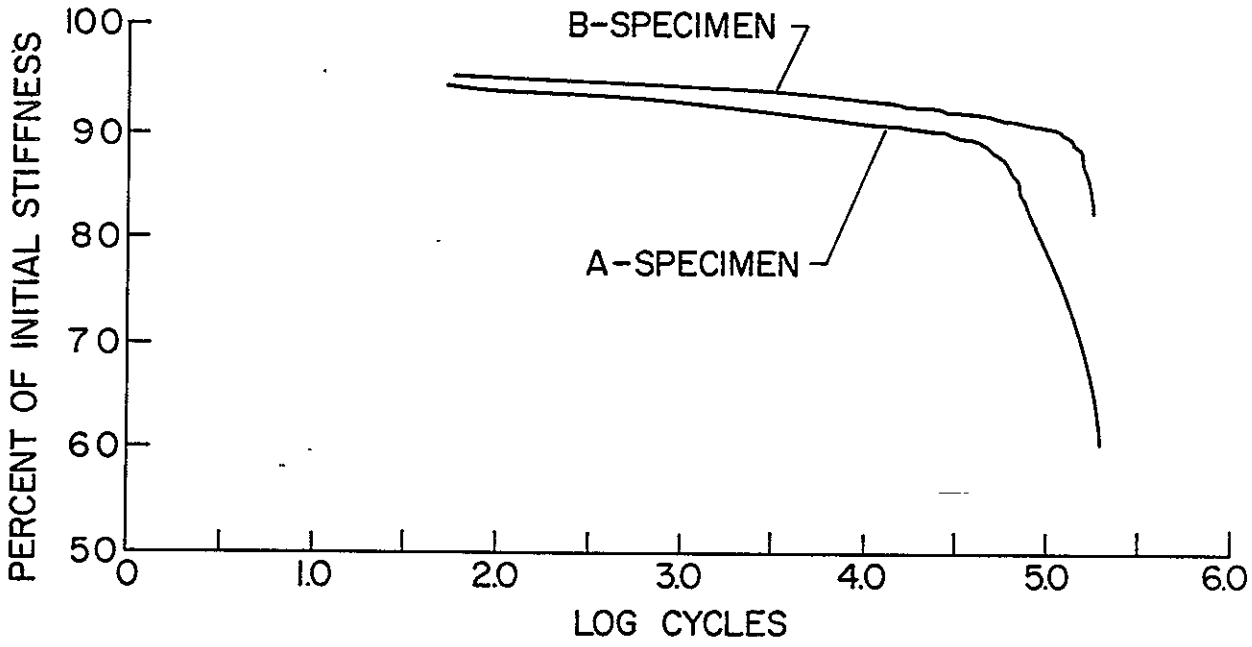

Figure 26: Stiffness Degradation Versus Logarithmic Cycles

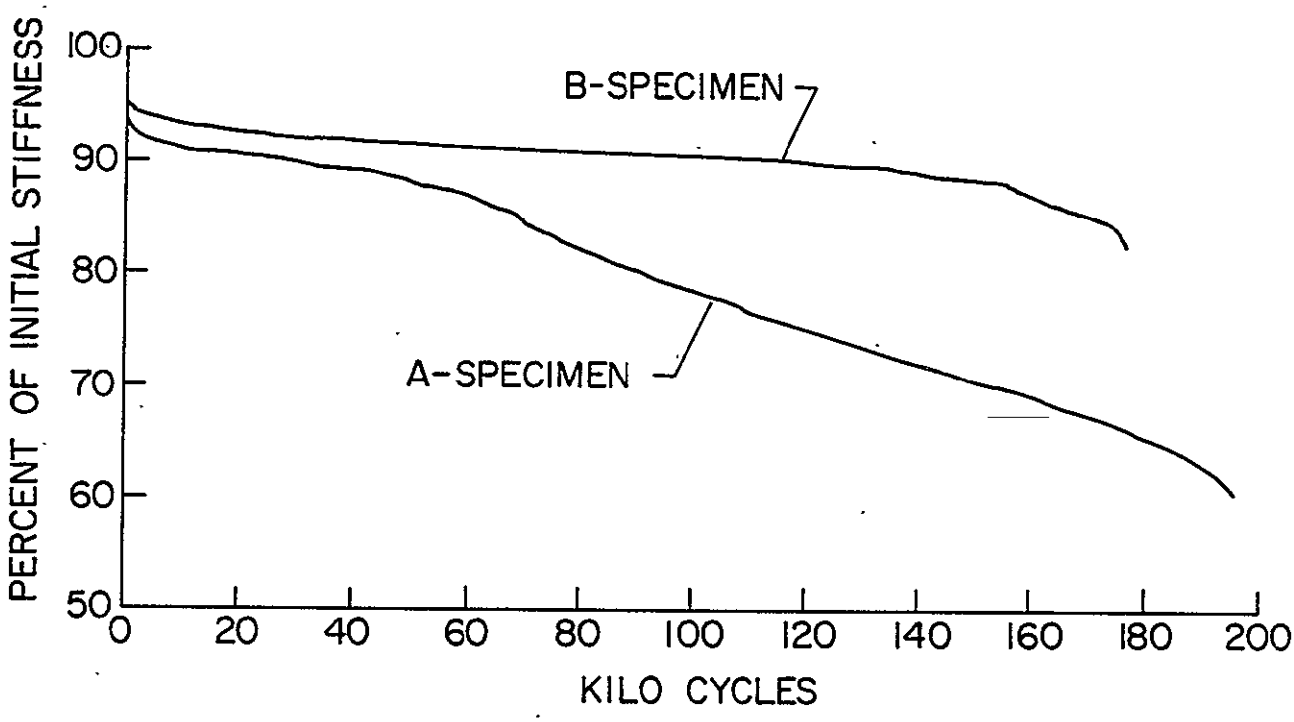

Figure 27: Stiffness Degradation Versus Linear Cycles

before failure is very great. Both laminates exhibit three sudden stiffness changes during the fatigue life: the first one occurs during the very first few cycles of loading, the second one occurs within the first half of the lifetime for the A-specimen and well before failure for the B-specimen, and the third, sudden stiffness loss leads to the failure of the specimens. The A-specimen has its second sudden stiffness loss at 70 k cycles and the corresponding event in the B-specimen occurs at 157 K cycles. Both events coincide with the onset of the knee in the logarithmically scale stiffness representation and are generally followed by an increased degradation rate.

It should be mentioned here that locally confined buckling effects were seen during cyclic loading of the A-specimen. On both sides of the specimen, the zero- and 90-deg sublaminate delaminated from the inner $[45,-45]_s$ group at locations governed by compressive circumferential stresses and buckled outwards. It could be hypothesized that the forming of these delaminations and the attendant stiffness degradation are rapidly accelerated after reaching a critical delamination size which facilitates buckling. The sudden stiffness change at 70 K for the A-specimen could then be related to the observed buckling effects. By visual inspection, no buckling effects were visible for the B-spec-

imen. However, at the end of fatigue life, it seemed to be apparent by visual observation that the surface 45-deg ply contributed little or nothing to the load transfer, since around the hole, matrix cracks were formed and some of the surface material confined by those cracks was almost completely delaminated. The matrix cracks prevent the in-plane load transfer and the delaminations make load transfer through interlaminar shear stresses impossible. These effects were visible at the end of the lifetime of the B-specimen, thus suggesting the possibility of a relationship between them and the sudden stiffness change at 157 K cycles. Finally it should be recalled that the 90 percent load levels for the A- and the B-specimens are represented by the maximum load values of 2354 lbs and 2195 lbs, respectively.

4.5 RESIDUAL STRENGTH

A number of the cyclic tests were halted at various stages of the loading history for nondestructive inspection of the damage zone and residual strength measurements. This series of tests provided a characteristic and repeatable curve of the change in residual strength throughout the loading history, Figures 25 and 28.

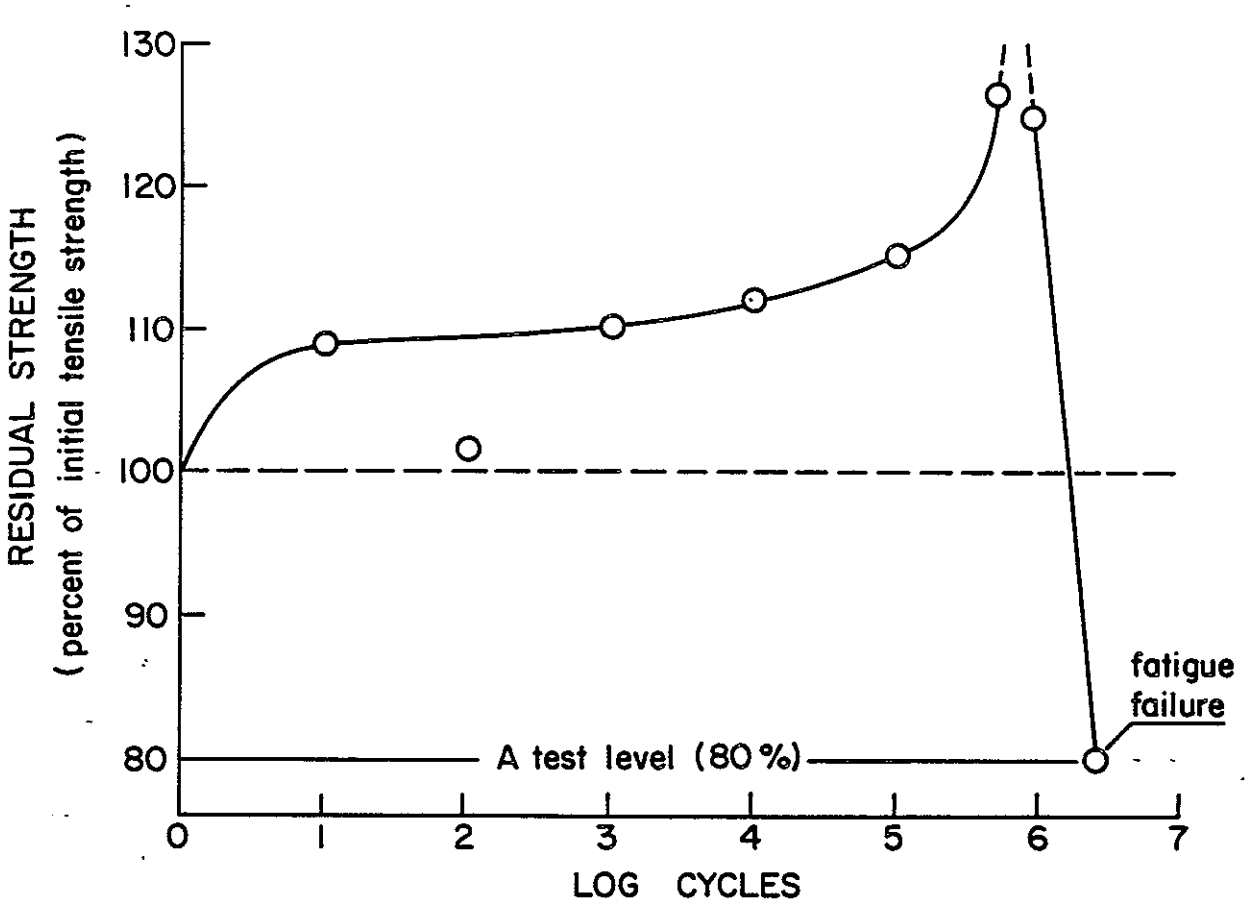

Figure 28: Residual Strength of an A-Laminate

During the first few (ten) cycles, the damage, primarily matrix cracks, reduces the effect of the stress concentration at the hole and the residual strength increase is on the order of ten percent. The actual strength increase does depend on the cyclic stress level, with the higher stress levels corresponding to slightly higher strength increases than the lower stress levels.

Stiffness change and residual strength data for a type B laminate after 100 cycles at a low cyclic stress amplitude are also shown in Figure 25. Both the increase in residual strength and the decrease in stiffness are less than those for the same type specimen cycled at the 85 percent stress level. The second region of the residual strength curve, approximately ten percent of the fatigue life, is characterized by a gradual, but constant rate of increase in residual strength over a logarithmic cycles scale. At the end of the second region, the increase in residual strength is 115 to 120 percent. The limits of regions I and II for residual strength are approximately the same as observed for stiffness change.

The third region of the residual strength curve is marked by a further increase in residual strength. Although the data in this region are incomplete, it appears that the maximum residual strength is reached between 50 and 80 percent

of the lifetime. The largest residual strengths are 126 and 142 percent of the initial strength for the type A and B laminates, respectively. During the final region of the fatigue life, the residual strength decreases until the strength equals the level of maximum cyclic stress, as shown in Figures 25 and 28. The last two regions of the residual strength-log cycles curve correspond to the third region of the stiffness reduction curve where the stiffness change shows a sharp decrease on the log cycles plot. The logarithmic scale used to represent the lifetime may cause some confusion in interpreting these results. The residual strength data have been replotted in Figure 29 using a linear scale to represent cycles.

4.6 DAMAGE PATTERNS

Static damage starts with matrix cracks usually in the surface plies at 1570 lbs load for the A-laminate and 1220 lbs load for the B-laminate. At higher load levels, cracks appear in all directions. The A-laminate develops more well defined zero-deg cracks tangent to the hole while the B-laminate develops more well defined 45-deg cracks. Note that these are the directions of the surface layers, respectively. In both laminates, 45-deg and zero-deg cracks are more well defined than -45-deg and 90-deg cracks. The lat-

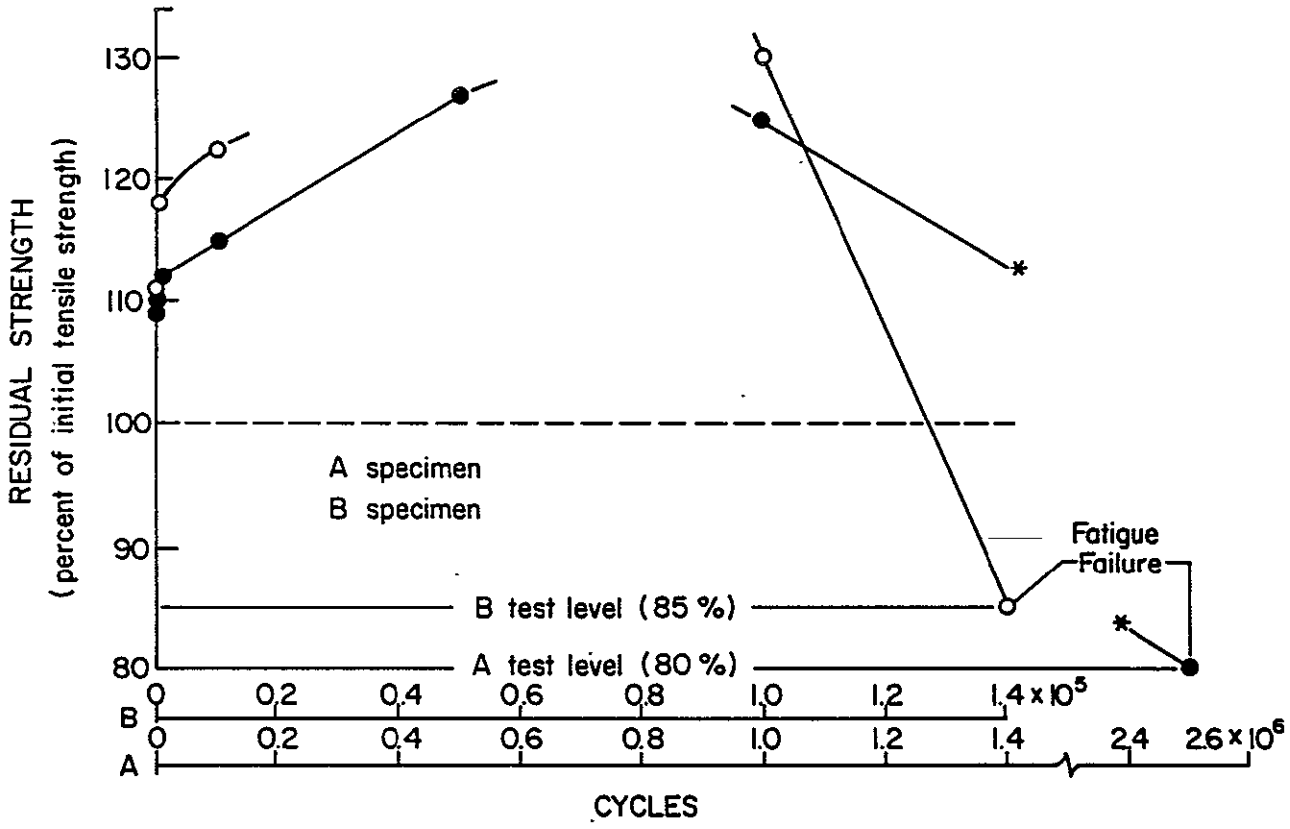

Figure 29: Residual Strength Versus Linear Cycles

ter cracks are often secondary cracks in the sense that they are initiated at locations where 45-deg and zero-deg cracks already exist. Zero-deg cracks in the A-laminate grow to a length of more than five hole diameters. When the tangent zero-deg cracks approach their maximum length, cracks in 45-deg and 90-deg direction are also initiated on the straight edge. In the final stages of lifetime, a regular pattern of matrix cracks is formed between the tangent zero-deg cracks and the straight edges. The uniformity of these cracks is similar to damage patterns of unnotched laminates, so-called characteristic damage states (CDS).

The delamination zone visible on an X-ray photo consists of the superimposed images of the delaminations on the various laminate interfaces. It seems as if the tangent zero deg cracks in both the A- and B-laminates are associated with delaminations on adjacent interfaces. Those delaminations have the largest continuously connected area of all delaminations in the laminates. In general, while the A-laminate develops a much larger delamination along its tangent zero-deg cracks, the more confined delaminations of the B-laminate spread along the 45-deg direction and reach the straight edge. It is emphasized that Figure 14 and Figure 15 give the spatial distributions and the characteristic shapes as well as the proper magnitude of the delamination

zones. Noting that the area of delaminations on all interfaces is higher for the A-laminate than for the B-laminate, we recall that the A-specimens experienced much higher stiffness losses during their fatigue life than the B-specimens.

The observations on the locations of initial delaminations in type A and B laminates presented in Sections 3.1.1.1 and 3.1.2.1 agree with the analysis of O'Brien and Raju [12]. However, the stress levels at which the delaminations initiated were lower than those predicted by the strain energy release rate analysis which considered delamination as the only damage mode. Experimental data for unnotched T300/5208 quasi-isotropic laminates by O'Brien [13] show that delaminations initiate in the laminates with matrix cracks at lower critical strain energy release rates than in laminates without matrix cracks. This observation is supported by the results of Jamison and Reifsnider [6] and Wang [14]. The fact that the measured strains at initiation of delamination in type A and B laminates, in which matrix cracking was the first damage mode, were lower than the initiation strains predicted by the analysis considering only delamination is consistent with other reported results. Matrix cracking is an important phase of the damage development process. Although matrix cracks, by themselves, may

not significantly affect the strength and life of structural laminates, they do act as catalysts to initiate other strength and life-limiting damage modes such as delamination and fiber fracture [6].

4.7 DAMAGE AND MECHANICAL RESPONSE

Figure 17 shows that the tangent zero-deg cracks have a strong redistributing effect on the strain field near the hole, reducing the maximum strain concentration in the longitudinal direction. Except at the crack tips, the strain distribution along the cracks is almost uniform. Figure 30 presents the average strain concentrations as a function of the length of the tangent cracks at various fatigue stages for the A-specimen. After 600K cycles, which is estimated as being 50 percent of the expected lifetime the strain concentration is reduced to $K_{\varepsilon}=1.46$.

Figure 31 shows the decrease of strain concentration versus the logarithmically scaled number of cycles. The rate of decrease is very high during the first cycles of fatigue loading. Recalling that the rate of increase of residual strength of both laminates is very high in the early stages of fatigue life, it seems very likely that the tangent zero-deg cracks are a main factor influencing residual strength.

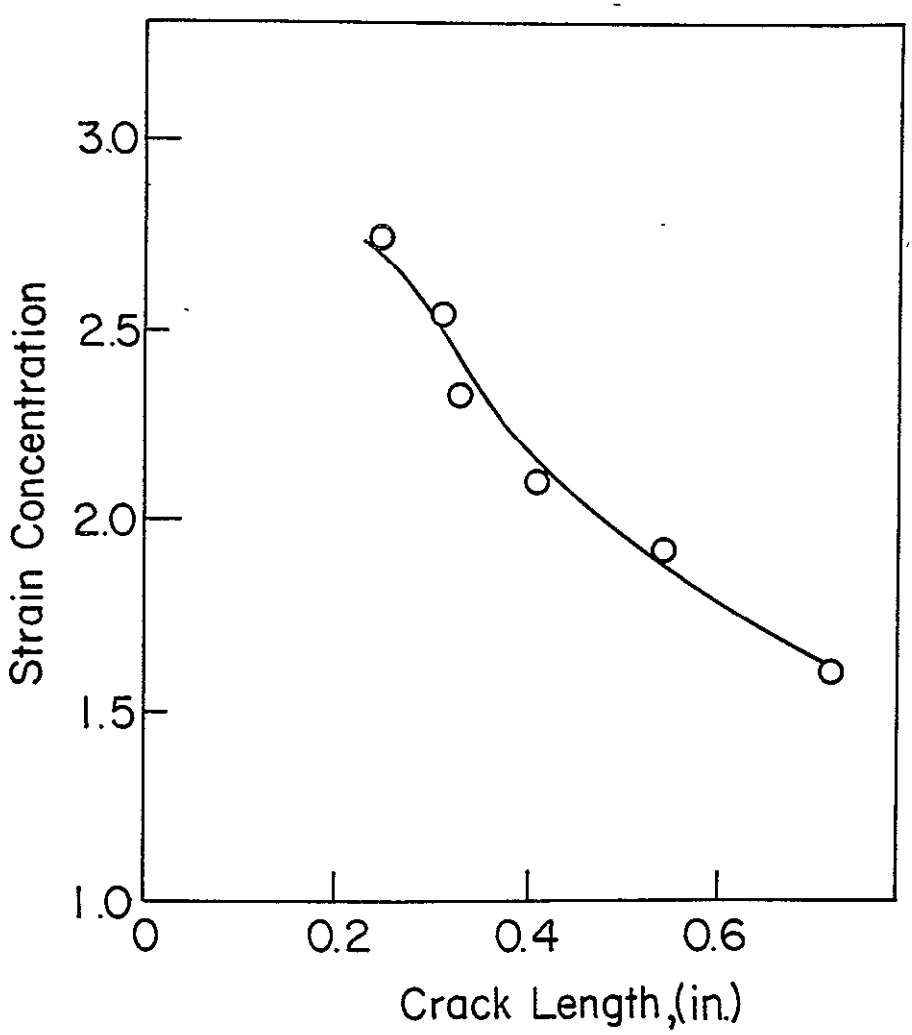

Figure 30: Strain Concentration Versus Crack Length for an A-Laminate

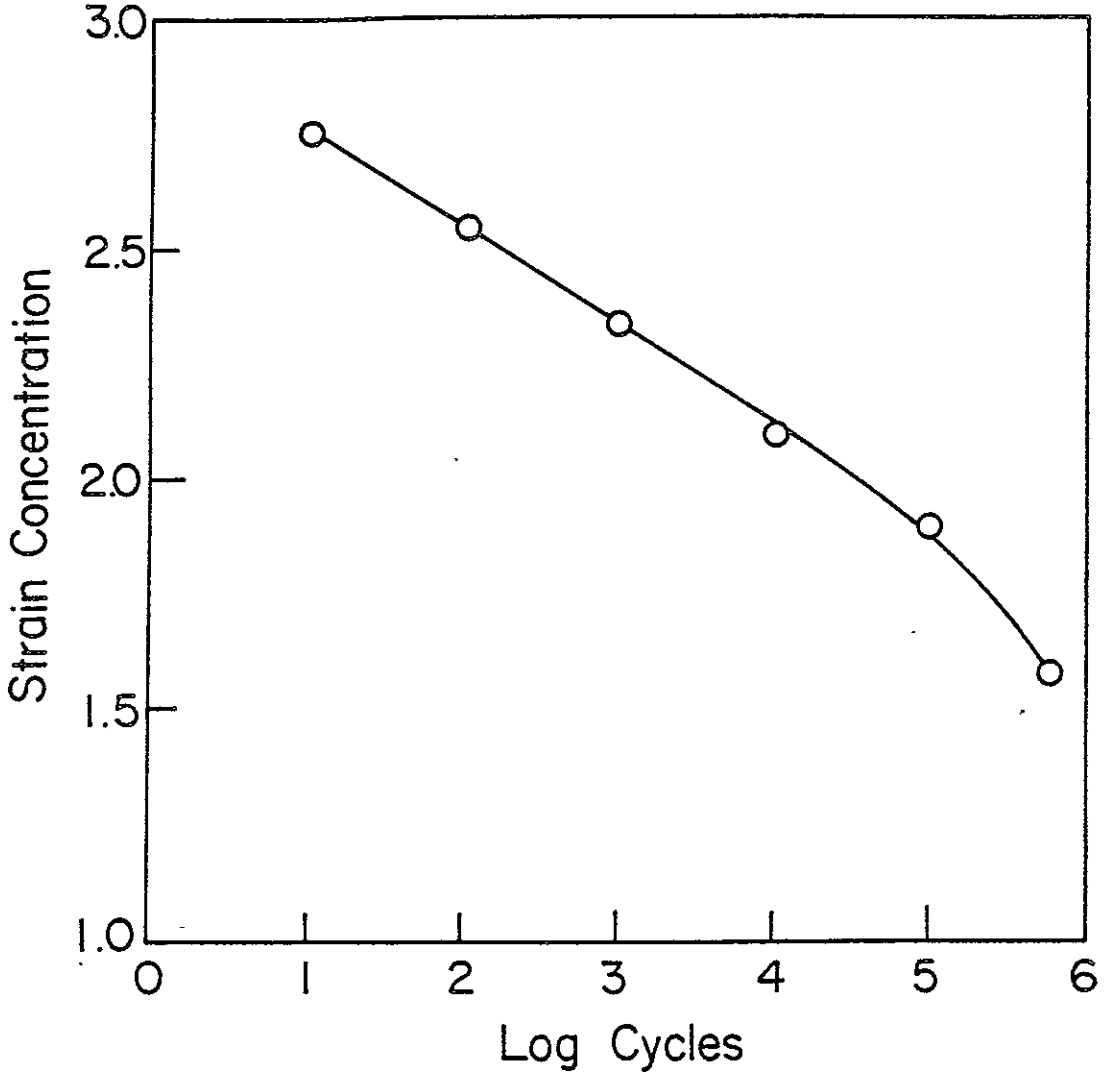

Figure 31: Strain Concentration Versus Cycles for an A-Laminate

Figure 32 shows the results of two strength tests performed on an A-specimen and a B-specimen versus the length of the tangential cracks obtained from X-ray photos taken after applying the fatigue load. Cracks of equal length in A- and B-specimens seem to influence the strength increases of A- and B-specimens differently. As a result of a linear curve fit for the data points, the increase in strength rate is 44 percent per inch for the B- and 23 percent per inch for the A-laminate.

A residual-strength versus strain-concentration curve (Figure 33) was constructed from the data used in Figure 30 and Figure 32 by eliminating the crack length. Figure 34 and Figure 35 show the increase in length of cracks in the zero-deg plies with the number of cycles under fatigue load. The crack lengths are the average values of the length of the two cracks visible on X-ray photos. For two reasons it is difficult, however, to measure average crack length exactly. First, the length of the dark line on a X-ray matches the actual crack length only in the case of complete penetration with zinc iodide. Second, it is difficult to decide what the length of a crack is since a dark line on a X-ray is the superimposed image of actually two cracks on each side of the laminate midplane. If these two actual cracks are shifted longitudinally, one might measure a

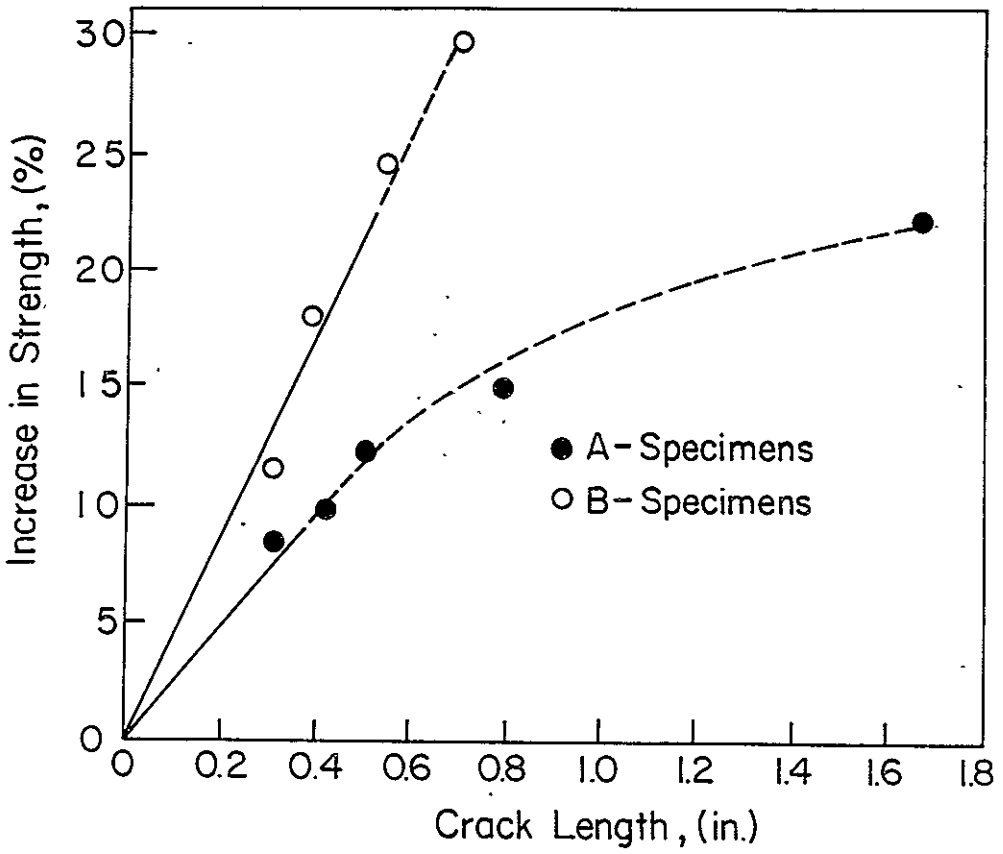

Figure 32: Residual Strength Versus Crack Length

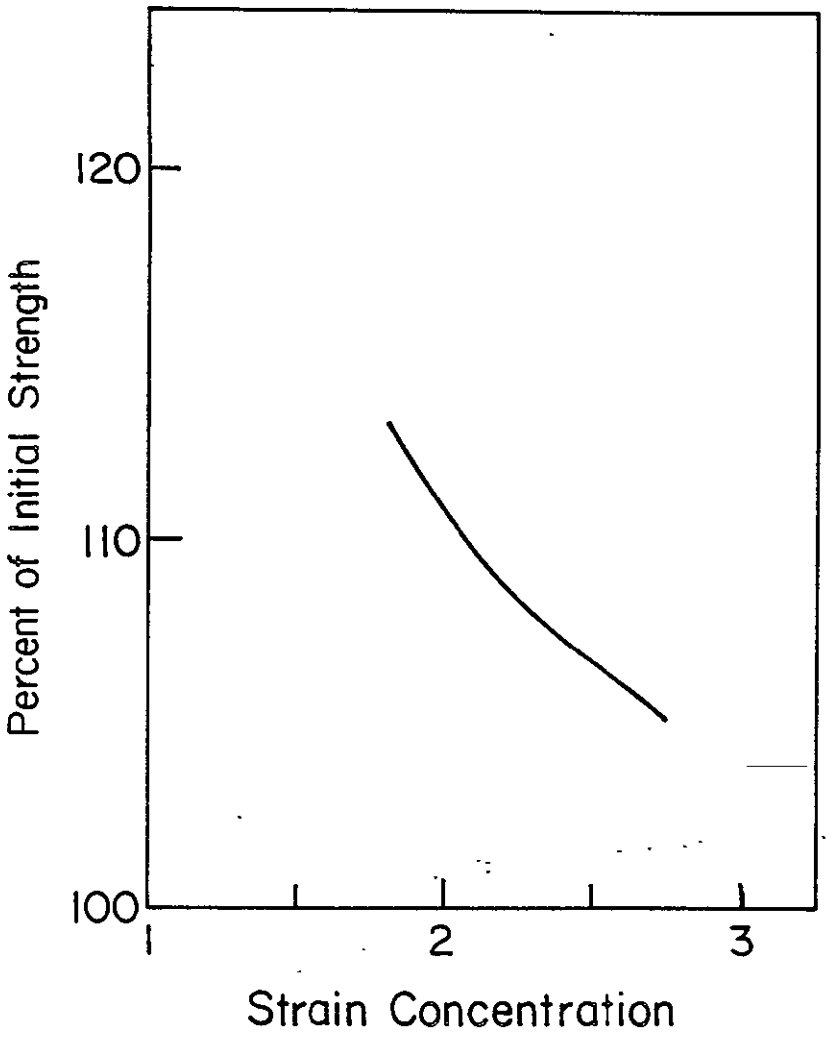

Figure 33: Strain Concentration Versus Residual Strength

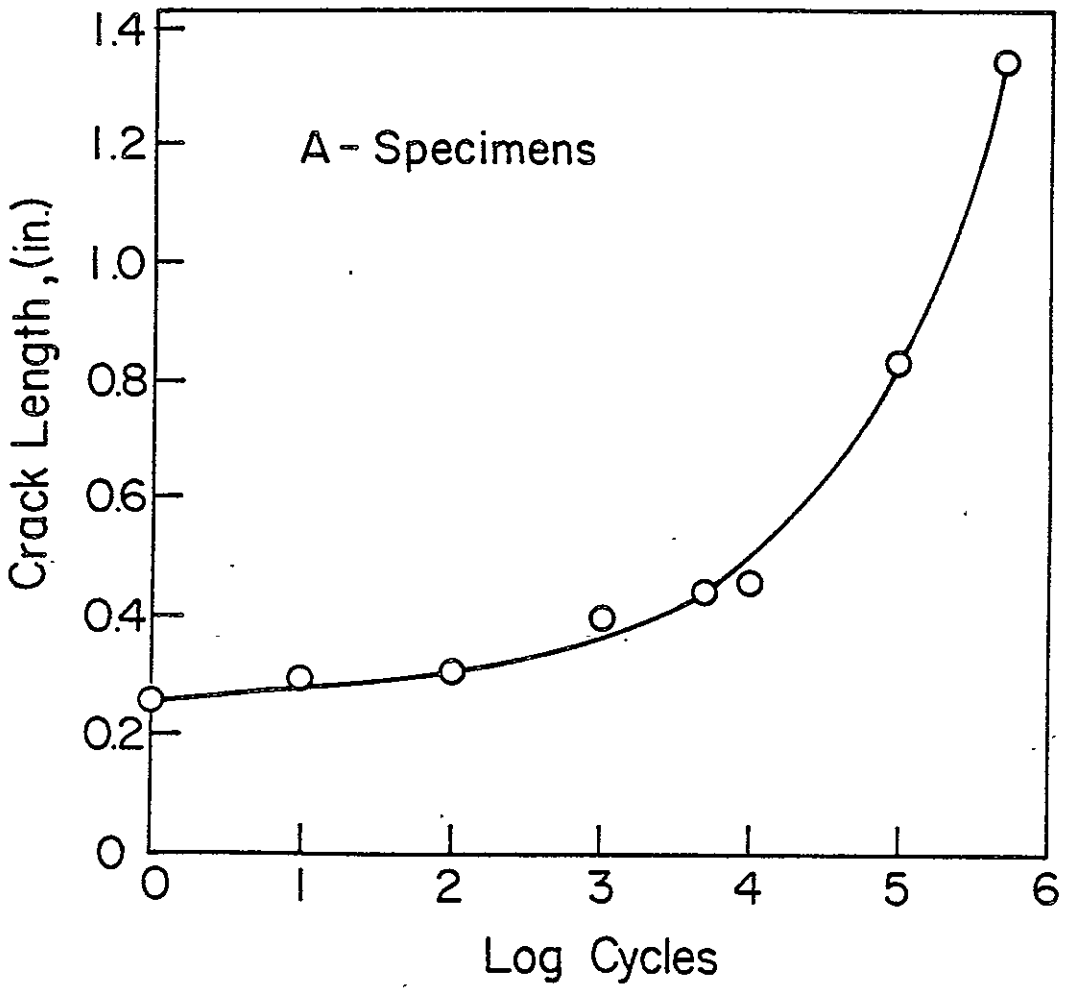

Figure 34: Zero-Deg Crack Length Versus Number of Cycles for an A-Laminate

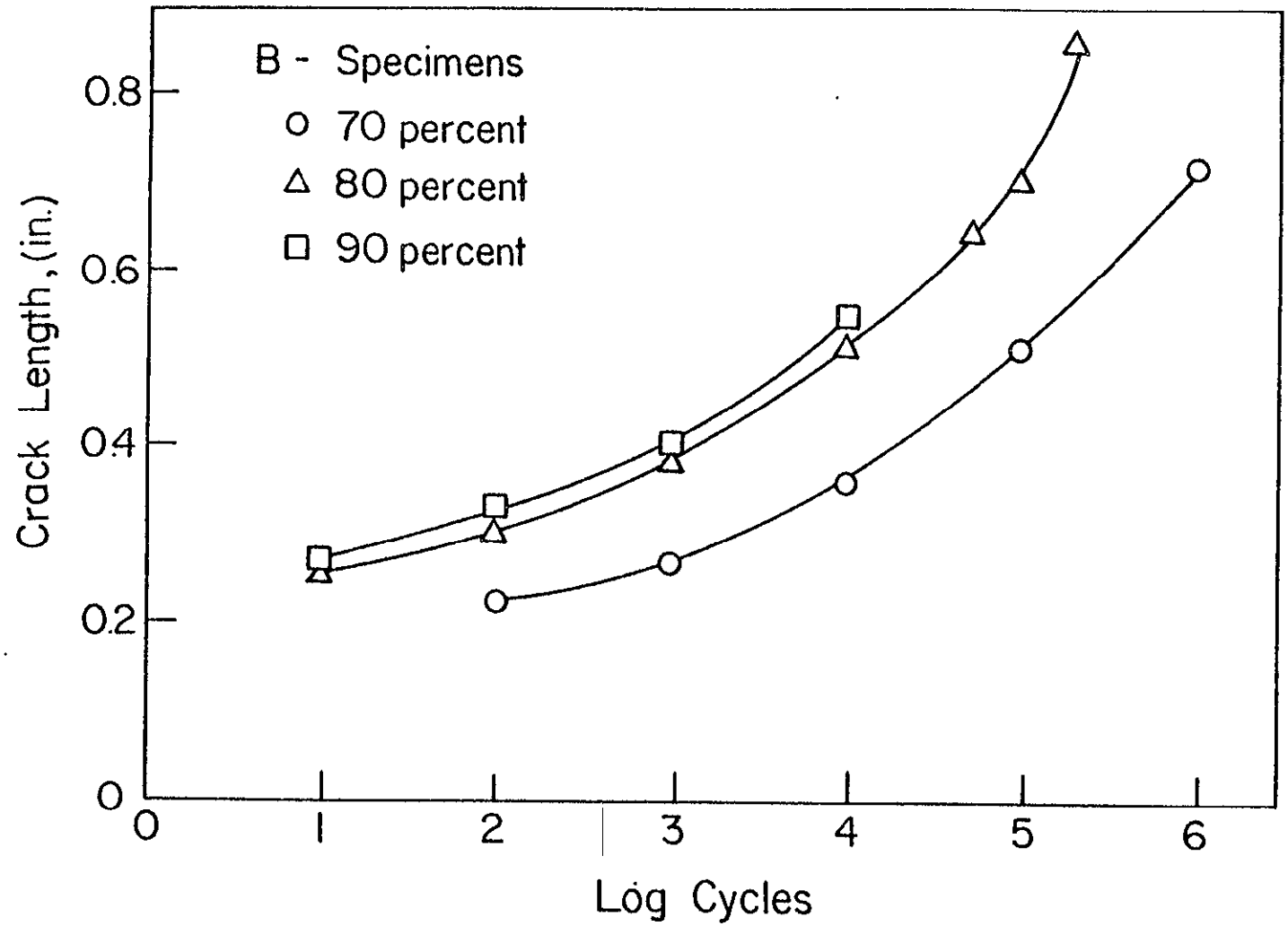

Figure 35: Zero-Deg Crack Length Versus Number of Cycles for B-Laminates

longer crack length than actually exists. Since the data for the B-laminate is more complete, Figure 35 provides information on the influence of the load parameter on the growth rate of those cracks. Figure 34 takes into account the initial crack length due to static load.

The appearance of the fracture surfaces depends on the subcritical damage in the specimens and the loading history. Several failed type A and type B specimens are shown in Figures 36 and 37, respectively. A typical fracture due to monotonic tensile loading is located along a straight line passing through the center of the hole as shown in Figures 36a and 37a. During cyclic loading, the damage zones, consisting of matrix cracks and delaminations, are larger and less localized than the concentrated damage zones caused by a monotonic tensile load. Failures due to monotonic loading after a period of cyclic loading are shown in Figures 36b and 37b and are less regular than those due to only monotonic loading. Cyclic loading to fracture causes the damage zones to extend away from the region of the hole, creating a highly irregular fracture pattern as shown in Figures 36c and 37c.

The phenomenon of irregular fracture surfaces, as shown in Figures 36 and 37, for specimens with long loading histories, can be related to the shift of high strain concentrations away from the hole. Since those strain concentrations are

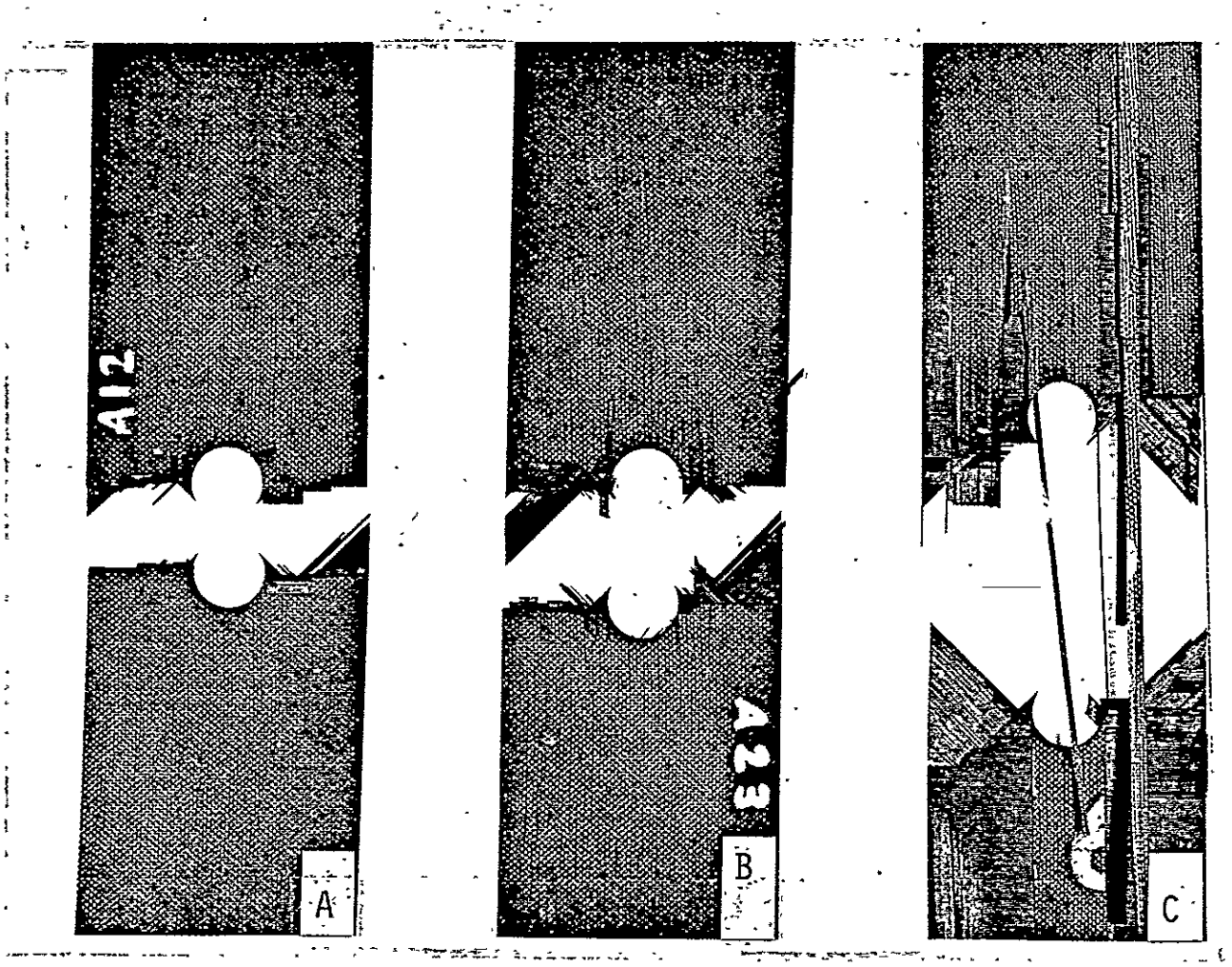

Figure 36: Fracture Surfaces of Type A Laminates: (a) monotonic tension, no prior damage; (b) monotonic tension after 500,000 cycles at $\sigma_{max} = 0.8\ \sigma_{ult}$; and (c) fatigue failure after 1.3 million cycles at $\sigma_{max} = 0.8\ \sigma_{ult}$.

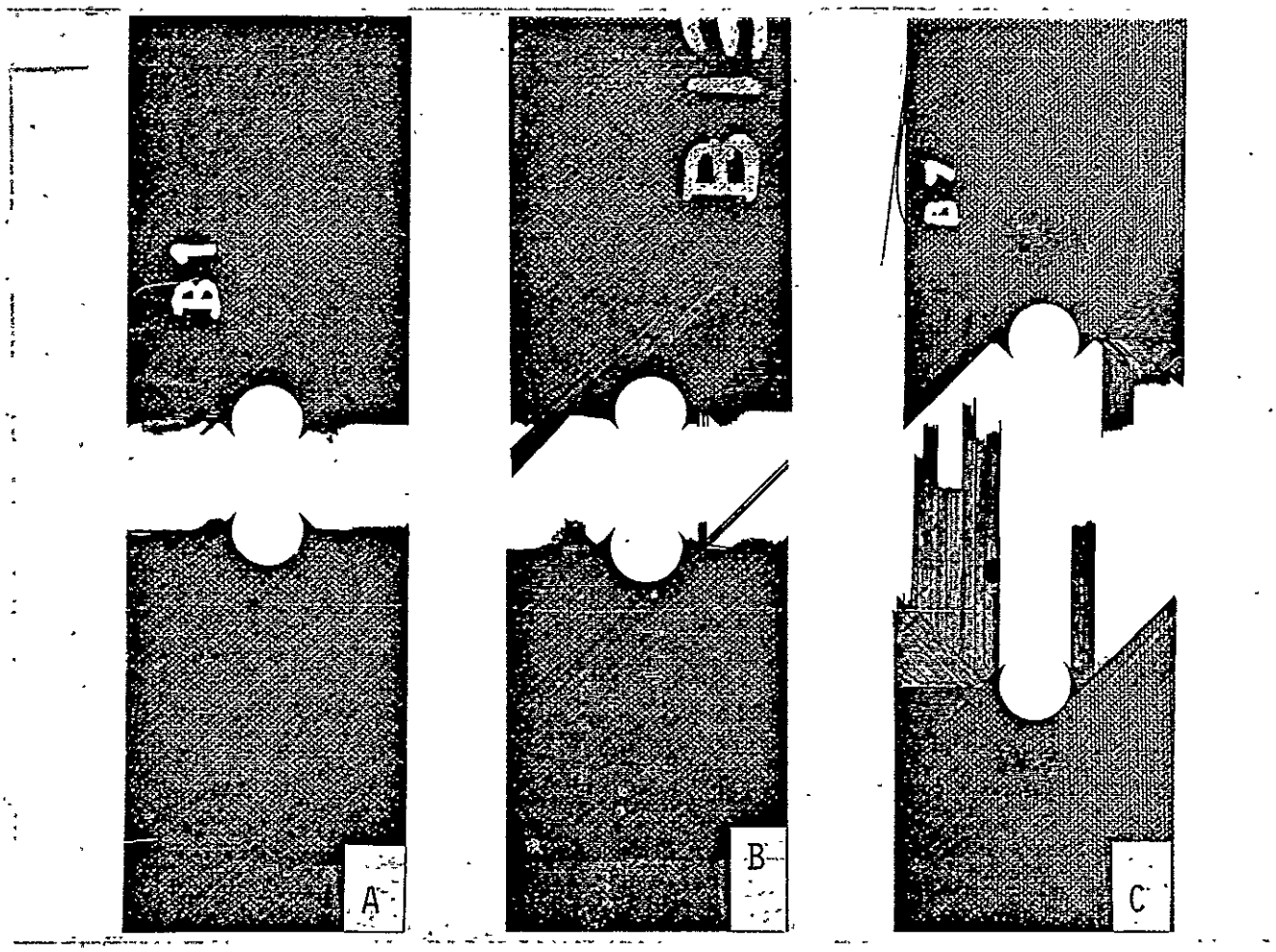

Figure 37: Fracture Surfaces of Type B Laminates: (a) monotonic tension, no prior damage; (b) monotonic tension after 200,000 cycles at $\sigma_{max} = 0.8\ \sigma_{ult}$; and (c) fatigue failure after 220,000 cycles at $\sigma_{max} = 0.8\ \sigma_{ult}$.

presumably highest at the tips of the cracks, we conclude that catastrophic failure can be initiated there. Specimen A-6 underwent a fatigue life test at the 80 percent load level and its fracture surface is shown in Figure 36c. Many zero-deg fibers broke at a distance from the hole of 6 to 7 hole diameters or from 2.2 inches to 2.6 inches. As for the phenomenon of stiffness degradation, we note that the A-laminate exhibits much larger delaminations than the B-laminate. These delaminations and also the buckling described in the section on continuous stiffness recording contribute to higher stiffness losses in the A-laminate than in the B-laminate.

5.0 CONCLUSIONS

1. Enhanced X-ray radiography gives detailed information on matrix cracks that can be used to establish relations between the location and length of the cracks and the fatigue response of laminates.

2. In conjunction with X-ray radiography, the deply technique gives the shape, size, and spatial distribution of delaminations.

3. The moire technique can be used to detect damage in the surface layer and related effects in the displacement field. Local stiffness can be measured for various damage situations. These results are in good agreement with extensometer measurements. The moire patterns of the laminate with the zero-deg surface layer (type A) gave more evidence about relations between damage and response than those of the B-laminate. All possibilities of the moire technique were not completely used in this work. More sophisticated data processing methods could help to take full advantage of this technique.

4. Stiffness losses during the lifetime are dependent on load levels and reached 20 percent for the B-laminate and 40 percent for the A-laminate. Stiffness-change versus number-of-cycles curves are typical for each laminate.

5. Residual strength exceeds initial strength until the final stages of lifetime are reached. Increases may reach levels of at least 26 percent for the A- and 42 percent for the B-laminate. Laminates with the higher initial strength are not necessarily those with higher residual values.

6. The pre-failure damage patterns, consisting of matrix cracks and delaminations are characteristic for each laminate. In general, surface layer matrix cracks associated with the hole develop sooner and extend further than the matrix cracks in the other layers. Delaminations can be caused by certain stress situations in the undamaged or low damaged specimen as well as by stresses which are due to the presence of matrix cracks. Delaminations between the surface layer and the adjacent layer followed major cracks in the surface layer. Moreover, tangent zero-deg cracks are well defined in both laminates and are associated with

delaminations on adjacent interfaces. In the A-specimen, these delaminations cover a larger area than the other delaminations. In the B-specimen, the wing-like delaminations between the 45-deg surface layer and the adjacent 90-deg layer extend further but do not necessarily cover a larger area than the delaminations between the zero-deg and the adjacent -45-deg layer. Since the zero-deg ply is a surface layer in the A-laminate, it has longer zero-deg cracks than the B-laminate and consequently the area covered by the delaminations initiated by these cracks is much larger than that for the B-specimen.

7. Zero-deg matrix cracks tangent to the hole have a major influence on residual strength via relaxation of strain concentrations near the hole. The relationship between crack length and residual strength is dependent on the stacking sequence. It appears that the length of zero-deg matrix cracks has a major influence on delamination size and attendant stiffness change. Further work could better quantify these relations.

8. The matrix cracks and delaminations which develop at the hole due to cyclic tension-tension loads change the geometry of the notch and reduce the strain concentration at the hole during the first 50 to 80 percent of the fatigue life. During this period, the residual tensile strength of the laminate increases. Throughout the remaining portion of the fatigue life, damage continues to grow in the ligaments of material adjacent to the hole and reduces the strength of the ligaments. Fatigue failure occurs when the damaged ligaments cannot support the maximum cyclic load; i.e., when the strength is reduced to a value equal to the maximum applied cyclic tensile stress.

VI

6.0 REFERENCES

1. W. W. Stinchcomb and K. L. Reifsnider, "Fatigue Damage Mechanisms in Composite Materials: A Review," Fatigue Mechanisms, J. T. Fong, Ed., ASTM STP 675, American Society for Testing and Materials, 1979, pp. 762-787.

2. W. W. Stinchcomb, K. L. Reifsnider, P. Yeung, and J. Masters, "Effect of Ply Constraint on Fatigue Damage Development in Composite Material Laminates," Fatigue of Fibrous Composite Materials, ASTM STP 723, American Society for Testing and Materials, 1981, pp. 64-84.

3. G. P. Sendeckyj, G. E. Maddux, and E. Porter, "Damage Documentation in Composites by Stereo Radiography," Damage in Composite Materials, ASTM STP 775, K. L. Reifsnider, Ed., American Society for Testing and Materials, 1982, pp. 16-26.

4. S. M. Freeman, "Damage Progression in Graphite-Epoxy by a Deplying Technique," AFWAL-TR-81-3157, Wright Patterson Air Force Base, OH, Dec. 1981.

5. Daniel Post, "Optical Interference for Deformation Measurements -- Classical Holographic and Moire Interferometry," Mechanics of Nondestructive Testing, W. W. Stinchcomb, Ed., Plenum Press, New York, 1980.

6. R. D. Jamison and K. L. Reifsnider, "Advanced Fatigue Damage Development in Graphite Epoxy Laminates," AFWAL-TR-82-3103, Dec. 1982.

7. T. K. O'Brien, "Stiffness Change as a Nondestructive Damage Measurement," Mechanics of Nondestructive Testing, W. W. Stinchcomb, Ed., Plenum Press, New York, 1980.

8. E. T. Camponeschi and W. W. Stinchcomb, "Stiffness Reduction as an Indicator of Damage in Graphite/Epoxy Laminates," Composite Materials: Testing and Design (Sixth Conf.), ASTM STP 787, I. M. Daniel, Ed., American Society for Testing and Materials, 1982, pp. 225-246.

9. J. D. Whitcomb, "Experimental and Analytical Study of Fatigue Damage in Notched Graphite/Epoxy Laminates," Fatigue of Fibrous Composite Materials, ASTM STP 723, American Society for Testing and Mterials, 1981, pp. 48-63.

10. J. M. Whitney and R. J. Nuismer, "Stress Fracture Criteria for Laminated Composites Containing Stress Concentrations," J. Composite Materials, Vol. 8, July 1974.

11. J. M. Whitney and R. Y. Kim, "Effect of Stacking Sequence on the Notched Strength of Laminated Composites," Composite Materials: Testing and Design (Fourth Conf.), ASTM STP 617, American Society for Testing and Materials, 1977, pp. 229-242.

12. T. K. O'Brien and I. S. Raju, "Strain Energy Release Rate Analysis of Delamination Around an Open Hole in Composite Laminates," presented at the 25th AIAA/ASME/ASCE/AHS Structures, Structural Dynamics, and Materials Conference, Palm Springs, CA, May 1984.

13. T. K. O'Brien, "Mixed-Mode Strain Energy Release Rate Effects on Edge Delamination of Composites," Effects of Defects in Composite Materials, ASTM STP 836, D. Wilkins, Ed., American Society for Testing and Materials, 1984.

14. A. S. D. Wang, N. N. Kishore, and C. A. Li, "On Crack Development in Graphite-Epoxy $[0_2/90_n]_s$ Laminates Under Uniaxial Tension," to be presented at the International Symposium on Composites, Materials and Engineering, University of Delaware, Newark, DE, 1984.

VIRGINIA TECH CENTER FOR COMPOSITE MATERIALS AND STRUCTURES

The Center for Composite Materials and Structures is a coordinating organization for research and educational activity at Virginia Tech. The Center was formed in 1982 to encourage and promote continued advances in composite materials and composite structures. Those advances will be made from the base of individual accomplishments of the thirty-four founding members who represent ten different departments in two colleges.

The Center functions by means of an Administrative Board which is elected yearly. The general purposes of the Center include:

- collection and dissemination of information about composites activities at Virginia Tech,
- contact point for other organizations and individuals,
- mechanism for collective educational and research pursuits,
- forum and mechanism for internal interactions at Virginia Tech.

The Center for Composite Materials and Structures is supported by a vigorous program of activity at Virginia Tech that has developed since 1963. Research expenditures for investigations of composite materials and structures total well over five million dollars with yearly expenditures presently approaching two million dollars.

Research is conducted in a wide variety of areas including design and analysis of composite materials and composite structures, chemistry of materials and surfaces, characterization of material properties, development of new material systems, and relations between damage and response of composites. Extensive laboratories are available for mechanical testing, nondestructive testing and evaluation, stress analysis, polymer synthesis and characterization, material surface characterization, component fabrication and other specialties.

Educational activities include eight formal courses offered at the undergraduate and graduate levels dealing with the physics, chemistry, mechanics, and design of composite materials and structures. As of 1982, some 33 Doctoral and 37 Master's students have completed graduate programs and several hundred Bachelor-level students have been trained in various aspects of composite materials and structures. A significant number of graduates are now active in industry and government.

Various Center faculty are internationally recognized for their leadership in composite materials and composite structures through books, lectures, workshops, professional society activities, and research papers.

FOUNDING MEMBERS OF THE CENTER

Aerospace and Ocean Engineering
Raphael T. Haftka
William L. Hallauer, Jr.
Eric R. Johnson

Chemical Engineering
Donald G. Baird

Chemistry
James E. McGrath
Thomas C. Ward
James P. Wightman

Civil Engineering
Raymond H. Plaut

Electrical Engineering
Ioannis M. Besieris
Richard O. Claus

Engineering Science and Mechanics
Hal F. Brinson
John C. Duke, Jr.
Daniel Frederick
Robert A. Heller
Edmund G. Henneke, II
Carl T. Herakovich
Michael W. Hyer
Robert M. Jones
Manohar P. Kamat
Alfred C. Loos
Don H. Morris
Daniel Post
J. N. Reddy
Kenneth L. Reifsnider
C. W. Smith
Wayne W. Stinchcomb

Industrial Engineering and Operations Research
Joel A. Nachlas

Materials Engineering
David W. Dwight
D. P. H. Hasselman
Charles R. Houska
M. R. Louthan, Jr.

Mathematics
Werner E. Kohler

Mechanical Engineering
Norman S. Eiss, Jr.
Charles E. Knight
S. W. Zewari

Inquiries should be directed to:

Center for Composite Materials & Structures
College of Engineering
Virginia Tech
Blacksburg, VA 24061
Phone: (703) 961-4969

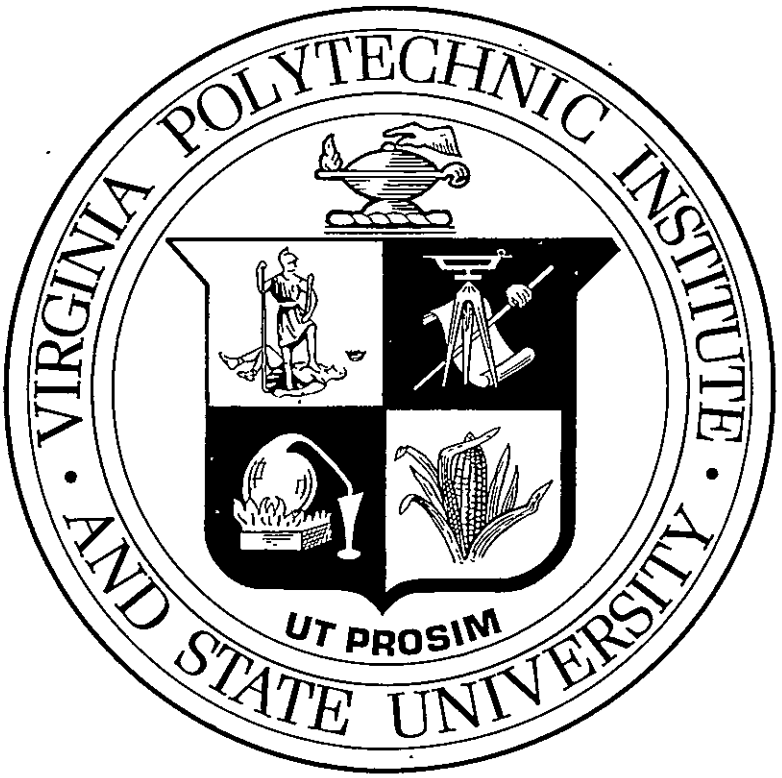
VIRGINIA POLYTECHNIC INSTITUTE
AND STATE UNIVERSITY
UT PROSIM